

AD732453

**SECOND QUARTERLY TECHNICAL REPORT
(1 April—30 June 1971)**

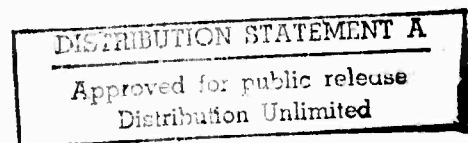
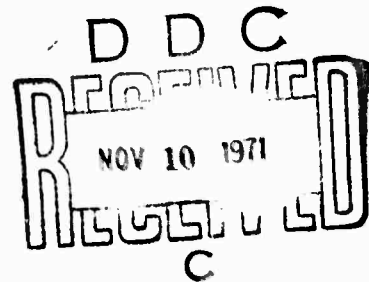
**USE OF ELECTRON BEAM GUN
FOR HARD ROCK EXCAVATION**

Submitted to

**U.S. Department of Interior
Bureau of Mines
Twin Cities Mining Research Center
Twin Cities, Minnesota
Contract No. H0110377**

Sponsored by

**Advanced Research Projects Agency
ARPA Order No. 1578
Program Code OF010**



**Westinghouse
Missile Launching & Handling Department
Sunnyvale, California**

Reproduced by
**NATIONAL TECHNICAL
INFORMATION SERVICE**
Springfield, Va. 22151

The views and conclusions contained in this document are those of the authors and should not be interpreted as necessarily representing the official policies, either expressed or implied, of the Advanced Research Projects Agency or the U. S. Government.

Distribution of this document is unlimited.

63

DOCUMENT CONTROL DATA - R & D

(Security classification of title, body of abstract and indexing annotation must be entered when the overall report is classified)

1. ORIGINATING ACTIVITY (Corporate author) WESTINGHOUSE ELECTRIC CORPORATION Missile Launching & Handling Department Hendy Avenue, Sunnyvale, California		2a. REPORT SECURITY CLASSIFICATION Unclassified	
		2b. GROUP ---	
3. REPORT TITLE USE OF ELECTRON BEAM GUN FOR HARD ROCK EXCAVATION —Second Quarterly Technical Report			
4. DESCRIPTIVE NOTES (Type of report and inclusive dates) Quarterly Technical Report (1 April - 30 June 1971)			
5. AUTHOR(S) (First name, middle initial, last name) David R. Nixon; Dr. Berthold W. Schumacher			
6. REPORT DATE 30 July 1971	7a. TOTAL NO. OF PAGES 40	7b. NO. OF REFS 10	
8a. CONTRACT OR GRANT NO. H0110377	9a. ORIGINATOR'S REPORT NUMBER(S) WEC R71-35		
b. PROJECT NO ARPA Order No. 1578	9b. OTHER REPORT NO(S) (Any other numbers that may be assigned this report)		
c. Program Code OF10			
d.			
10. DISTRIBUTION STATEMENT Distribution of this document is unlimited.			
11. SUPPLEMENTARY NOTES		12. SPONSORING MILITARY ACTIVITY Advanced Research Projects Agency Washington, D.C. 20301	
13. ABSTRACT An electron beam gun (EBG), which is not funded by the contract, is operational at low power and will be shipped to the field site in 4 to 6 weeks. Design and manufacturing effort on the EBG carriage was completed in June, and the carriage is undergoing preliminary operational and calibration tests. The Raymond Granite Company's quarry, located near Yosemite National Park, has been selected as the test site, because it has extensive sources of unfractured rock. A mathematical model has been developed that can describe the piercing of the rock by the electron beam and the thermal stresses subsequently produced. Trends in the time development of the calculated stress fields confirm laboratory observations for at least one geometry.			

14 KEY WORDS	LINK A		LINK B		LINK C	
	ROLE	WT	ROLE	WT	ROLE	WT
Electron Beam						
Tunneling						
Mining						
Rocks						
Minerals						
Excavation						
Fracture Mechanics						
Evaporation						
Melting						
Thermal Stress						

Distribution of this document is unlimited.

R 71-35
30 July 1971

SECOND QUARTERLY TECHNICAL REPORT
(1 April - 30 June 1971)

USE OF ELECTRON BEAM GUN
FOR HARD ROCK EXCAVATION

Contract No. H0110377

ARPA Order No. 1578
Program Code OF010

Effective Date of Contract: 11 December 1970
Contract Expiration Date: 10 December 1971
Amount of Contract: \$240,000 (CPFF)

Principal Investigator: D. R. Nixon
(408) 735-2271

Project Scientist: Dr. B. W. Schumacher
(412) 256-3522

WESTINGHOUSE ELECTRIC CORPORATION
Missile Launching & Handling Department
Sunnyvale, California

The views and conclusions contained in this document are those of the authors and should not be interpreted as necessarily representing the official policies, either expressed or implied, of the Advanced Research Projects Agency or the U. S. Government.

Distribution of this document is unlimited.

Details of illustrations in
this document may be better
studied on microfiche

FOREWORD

This quarterly technical report, covering the period 1 April - 30 June 1971, was prepared by the Westinghouse Electric Corporation. Special recognition is due Dr. R. C. Smith, of the Research Laboratories, who worked out the theoretical analysis in Section 4.

The research reported in this document is supported by the Advanced Research Projects Agency of the Department of Defense and is monitored by the Bureau of Mines under Contract H0110377.

CONTENTS

<u>Section</u>		<u>Page</u>
	ILLUSTRATIONS	iv
	TABLES	iv
	SUMMARY	v
1	INTRODUCTION	1-1
2	ELECTRON BEAM GUN AND SUPPORT EQUIPMENT	2-1
	2.1 Electron Gun and Controls	2-1
	2.2 Support Equipment	2-1
	2.2.1 Carriage Tests	2-1
	2.2.2 Modifications	2-7
3	FIELD TESTS	3-1
	3.1 Test Site Selection	3-1
	3.2 Site Support Equipment	3-4
	3.2.1 Electron Beam Gun Power Supplies	3-4
	3.2.2 Radiation Studies	3-4
4	THEORETICAL STUDIES	
	4.1 Piercing with Electron Beam	4-1
	4.2 Development of Thermal Stresses with Time	4-1
	4.3 Cavity Model	4-2
	4.4 Temperature Distribution	4-3
	4.5 Thermal Stress Calculations	4-9
	4.6 Interpretation of Stress Fields	4-16
	4.7 Rock Failure	4-19
5	LABORATORY TESTS	5-1
6	REFERENCES	6-1
	Document Control Data - R&D	

ILLUSTRATIONS

<u>Figure</u>	<u>Page</u>
2-1 Carriage with Mock-up of Electron Beam Gun (Front View)	2-3
2-2 Carriage with Mock-up of Electron Beam Gun (Right Side View)	2-4
2-3 Time Exposure with Light Attached to End of Simulated Transfer Column During Translation	2-5
2-4 Control Panel for Electron Beam Gun Carriage	2-6
3-1 Artist's Concept of Test Site Shield Structure	3-6
4-1 Time for Which Heat Flow Takes Place in Any Plane Perpendicular to Z-axis	4-5
4-2 Calculated Isotherms Using Simple Model with Cavity Boundary at 1700°C	4-6
4-3 Distance of Temperature Penetration into Rock Below End of Cavity as Function of Piercing Time	4-8
4-4 Finite Element Triangular Meshes: (a) Computer Run 2.1 (5 seconds) (b) Computer Run 2.6 (300 seconds)	4-10
4-5 Calculated Azimuthal Tension (θ Stress) for Piercing Times of 5, 10, 20, 40, 80, and 300 seconds	4-11
4-6 Calculated Maximum Principal Stress (Tension) in R-Z Plane for Piercing Times of 5, 10, 20, 40, 80, and 300 Seconds	4-12
4-7 Calculated Azimuthal Compression for Piercing Times of 5, 10, 20, 40, 80, and 300 Seconds	4-13
4-8 Calculated Minimum Principal Stress (Compression) in R-Z Plane for Piercing Times of 5, 10, 20, 40, 80, and 300 Seconds	4-14
4-9 Pink Jasper Quartzite Cracked after 9 Seconds of Piercing with 9-kW Beam (from Ref. 2)	4-18
4-10 Failure Probability Due to Tensile Stresses	4-20

TABLES

<u>Table</u>	<u>Page</u>
4-1 Parameter Values for Depth vs. Time Function (9-kW, 150-kV Electron Beam Gun)	4-2
4-2 Elastic and Thermal Parameters Assigned to Each Element According to Its Temperature	4-15

SUMMARY

PURPOSE

Westinghouse is seeking field operating data with which to verify and extend theoretical and laboratory data on the feasibility of employing the electron beam gun (EBG) to satisfy the needs for removal of hard rock. These practical data will provide initial definition of equipment configuration and applicable modes of operation.

TECHNICAL PROBLEMS

Support Equipment. Westinghouse is modifying its existing 36-kW EBG and will provide support equipment necessary for field operation.

Field Tests. This program involves the use of the 36-kW EBG to determine whether laboratory test data on melting rates, breakage mechanisms, etc., can be extrapolated to predict field performance. The field site being selected will provide working faces representative of a large, relatively unfractured rock mass. During field tests, Westinghouse will determine the techniques and procedures, such as cutting pattern, gun tracing speed, and method of cut, required to produce the optimum excavation rate.

Theoretical Studies. Westinghouse is studying the effects of different heating geometries and heating rates on stress distribution patterns and associated breakage phenomena. Westinghouse will also attempt to develop theoretical models for an optimum mode of operation.

Laboratory Tests. Westinghouse is conducting laboratory tests to support theoretical work and field experiments and to extend the use of the EBG to different rock types.

Systems Analysis Study. Westinghouse will evaluate the feasibility of developing a hard rock excavation system using the EBG as the prime source of power for rock fragmentation.

TECHNICAL RESULTS

This report covers effort performed during the second quarter of the contract. This work is a continuation of that reported in the first quarterly report (Ref. 3)*. Work was performed in four of the five areas summarized above; the systems analysis study will not become active until the field test effort has been completed and evaluated. A sixth area (not included in the contract) is the completion of the 36-kW EBG and its conversion from a laboratory model to a field test version.

Support equipment. Design work and manufacturing effort for the EBG carriage were completed in June 1971. The carriage is presently undergoing a series of preliminary operational and calibration tests. Some deficiencies in carriage design were noted in these tests, but these are being corrected prior to installation of the 36-kW EBG. Additional tests will be conducted with the EBG installed and with operational field support equipment to verify system operation.

Field Tests. Field test activity in the second quarter of the contract has again been primarily in the area of site review and selection. The site previously selected, i.e., the Logan quartz-gabbro quarry, is no longer being considered. The Logan rock is extensively fractured and faulted and, therefore, was deemed geologically undesirable, although it met all other criteria for site selection. Another site has been selected, which fulfills the geological requirements and most other site criteria. This is the Raymond Granite Company's quarry in Raymond, California, which is about 25 miles south-southwest of Yosemite National Park.

Other activities in the area of field tests have been the preparation of a preliminary field test plan, the specification for and concept design of a radiation shield for field use, and specification and acquisition of other site support equipment, such as motor-generator systems, radiation monitoring and detection instrumentation, and the required site utilities.

*See list of references in Section 6.

The EBG as modified for rock cutting in the field (long-beam transfer section to reach into holes and crevices) is operational at low power. Some delays were encountered in going to the desired higher power levels, and consequently shipment to the field site was delayed. This should be accomplished in 4 to 6 weeks.

Theoretical Studies. A mathematical model has been developed that can describe the piercing of the rock by the electron beam and the thermal stresses which are subsequently produced.

Computer printouts have been obtained for the stresses after 5 to 300 seconds of piercing with a 9-kW beam. It is not easy to derive from these plots when and where the rock will crack, but trends in the time development of the stress field can be seen that confirm laboratory observations, at least for one particular geometry. Computations must now be extended to other types of rocks, power levels, and geometric conditions.

Laboratory Tests. No laboratory tests were performed during the second quarter.

DoD IMPLICATIONS

The primary DoD implication of a successful field test program is the potential to fragment and remove hard rock from any location without degrading the structural integrity of the parent rock from which it was removed.

Upon completion of the appropriate development program, the EBG system could be applied to rock-removal systems for programs such as

- Sanguine
- Cheyenne Mountain
- Minuteman
- Safeguard
- AEC testing

and probably a number of other applications. In addition, an operational EBG system would have applications to the programs of the Department of Transportation and other agencies.

It should be stressed, however, that a considerable development program will be required after the assumed successful field tests before an operational system can be delivered.

IMPLICATIONS FOR FURTHER RESEARCH AND DEVELOPMENT

Westinghouse believes that the current field test program will demonstrate the potential of the EBG for hard-rock fragmentation. Based on the successful completion of these tests, additional research and development effort can be envisioned in the following areas:

1. Additional tests in various types of open quarries and in underground mines.
2. Evaluation of EBG in conjunction with existing mining and tunneling equipment and as part of a total system design.
3. Improved knowledge of rock failure mechanisms.
4. Investigation of the use of ion beams with their reduced shielding requirements.
5. Increase in power and/or increase in electron acceleration voltage.
6. Real-time predictions of geologic conditions using existing optical and acoustic sensing technologies.

These areas of continuing investigation will augment a product development program that is aimed at the achievement of a system to satisfy government and industrial needs for hard-rock removal.

1. INTRODUCTION

Laboratory tests conducted by Westinghouse have shown that the electron beam gun (EBG) may be a promising tool for use in hard-rock excavation (Refs. 1 and 2)*. These tests have been conducted on small, unconstrained, laboratory test specimens weighing a few hundred pounds. Under the present contract, field tests are to be conducted to study the electron beam process on a semi-infinite, constrained rock mass, such as might be encountered in mining or tunneling operations.

The objectives of the electron beam gun evaluation program are:

1. To obtain field operating data.
2. To determine the effectiveness and economic feasibility of the electron beam gun compared with conventional methods of hard-rock excavation.
3. To determine practical optimums for equipment configuration and modes of operation.

In support of the foregoing effort, laboratory experiments and theoretical studies are being conducted to compute and, if possible, to predict the thermal stresses and the resultant rock fragmentation for various cutting strategies and electron beam parameters in different types of rock.

*See list of references in Section 6.

2. ELECTRON BEAM GUN AND SUPPORT EQUIPMENT

2.1 ELECTRON GUN AND CONTROLS

The electron beam gun (EBG) was described in the First Quarterly Report (Ref. 3). At this time the gun has been operated at 150 kv and a few kilowatts of beam power, but adjustment of the electron optics for beam guidance through the long-beam transfer section at high power has not been completed. Unfortunately, this has delayed the start of the field tests.

2.2 SUPPORT EQUIPMENT

Support equipment for the EBG consists of the gun carriage, the vacuum system, and the electrical power supply system. Except for the motor-generator sets required in field operations, the vacuum system and electrical system existed as laboratory equipment prior to start of work under this contract. Thus, the principal task in this area is the design and manufacture of a carriage to support, position, and manipulate the gun during field test operations. The design task was completed in April 1971. A complete design description appeared in the First Quarterly Report (Ref. 3, p. 2-6). The manufacturing portion of the task was begun, and the completed carriage was delivered to Westinghouse in mid-June 1971.

Work on the carriage since delivery has consisted of completing the electrical and control systems, conducting an operational test of the carriage, and making minor modifications as a result of deficiencies observed in the tests. These tests and modifications are described below.

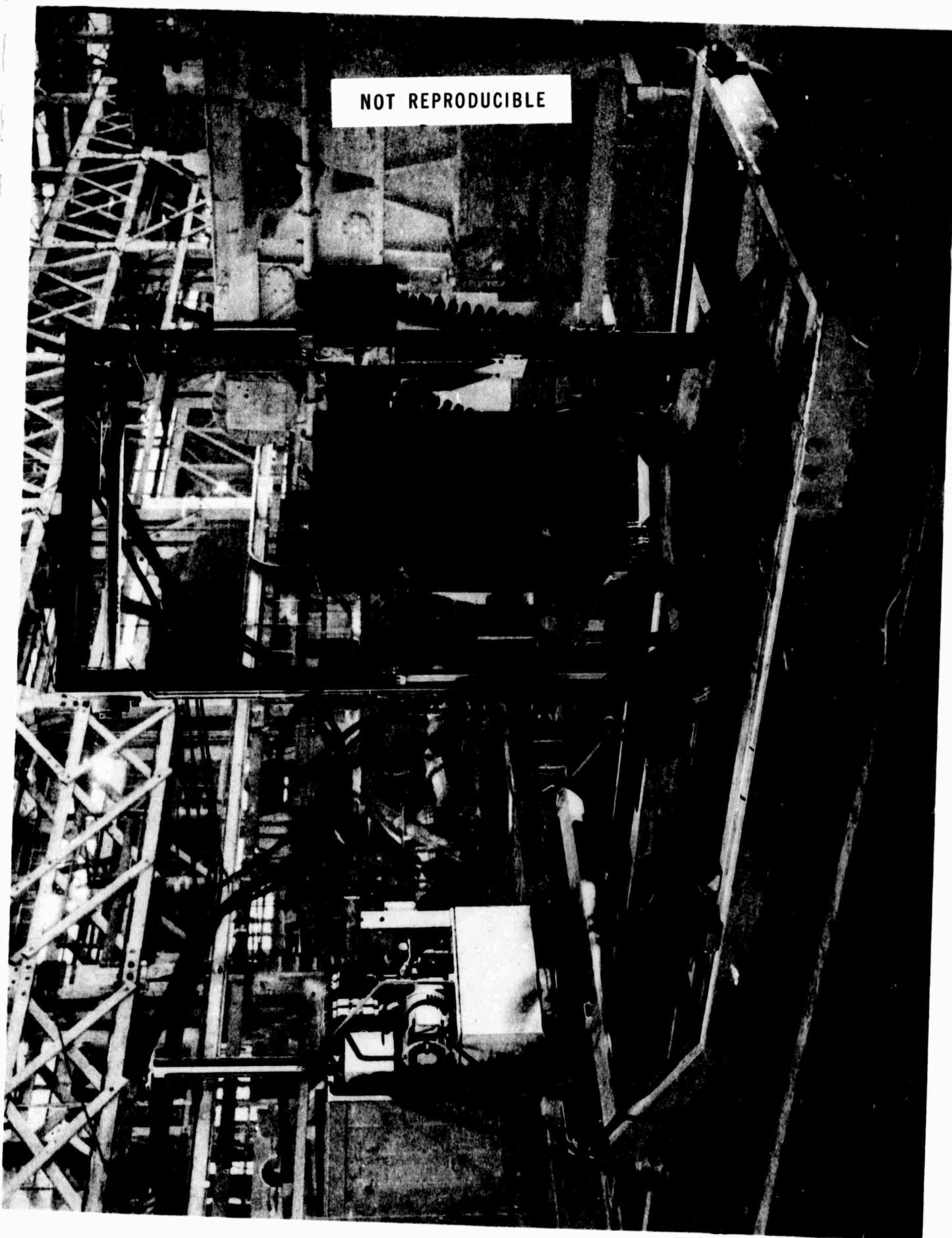
2.2.1 Carriage Tests

In-plant testing of the EBG carriage is subdivided into two categories: (1) an initial phase using a mock-up of an EBG, and (2) a final phase to verify operation of the carriage in conjunction with the 36-kW EBG.

The initial phase of the in-plant tests consists of several tests to verify operation of the carriage hydraulic system, to obtain calibration data for the system velocity controls, and to detect and measure any beam oscillations that might occur as a result of hydraulic transients or structural vibrations. Preliminary carriage tests were performed in a no-load condition to verify operation of all components. A concrete and steel pipe mock-up of the EBG was then constructed and mounted on the carriage for the remaining tests. The mock-up gun approximates the field test gun in space envelope, weight, and center-of-gravity location. The carriage, with the mock-up gun installed, appears in Figures 2-1 through 2-3. Figure 2-3 is a time exposure taken during carriage translation with a light attached to the end of the transfer column to record the gun motion. Although all modes of operation are represented in Figure 2-3, these motions do not extend to the limits of the gun manipulator. The control panel for the carriage is shown in Figure 2-4i.

After installation of the mock-up, a series of calibration tests was run to obtain the data required for velocity control. Each portion of the carriage hydraulic system is equipped with temperature- and pressure-compensated variable flow control valves. These valves will permit repeatable and constant velocity control for each mode of operation. The calibration consists of operating the various portions of the hydraulic circuit at several flow control settings. The actuation time for each operation is recorded and the results plotted as beam velocity vs. valve setting. These tests will be completed in early July.

The second phase of testing will begin when the 36-kW gun is installed on the carriage. This phase is comprised of a series of tests to recheck the previous valve calibration data, to identify any physical interference problems that may exist, and to verify operation of the EBG with the field configuration of vacuum pumps and motor-generator sets. The operational tests will include some preliminary cutting tests, to be performed using a 6 x 6 x 5-foot granite test block.



NOT REPRODUCIBLE

Figure 2-1. Carriage with Mock-up of Electron Beam Gun (Front View)

NOT REPRODUCIBLE

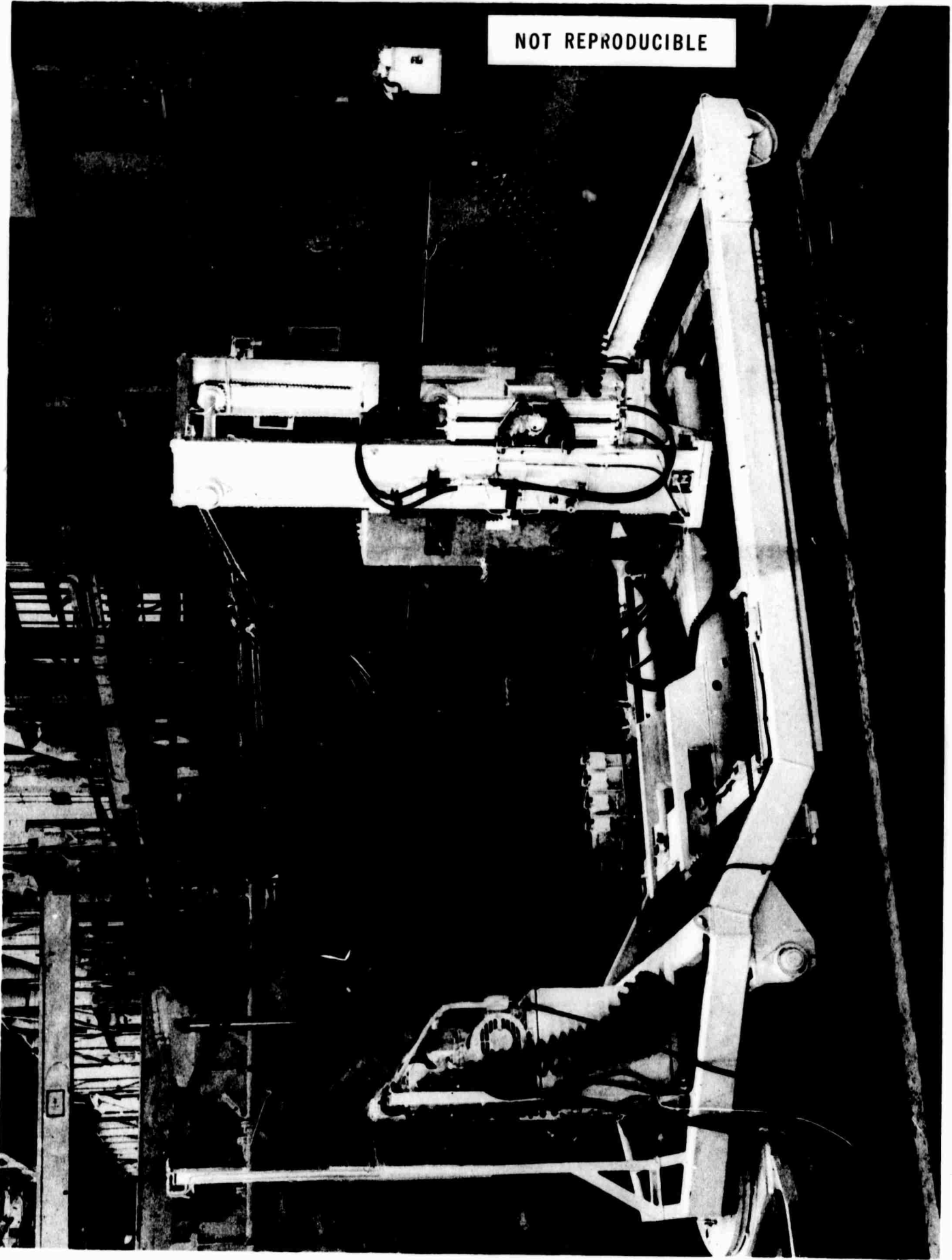


Figure 2-2. Carriage with Mock-up of Electron Beam Gun (Right Side View)

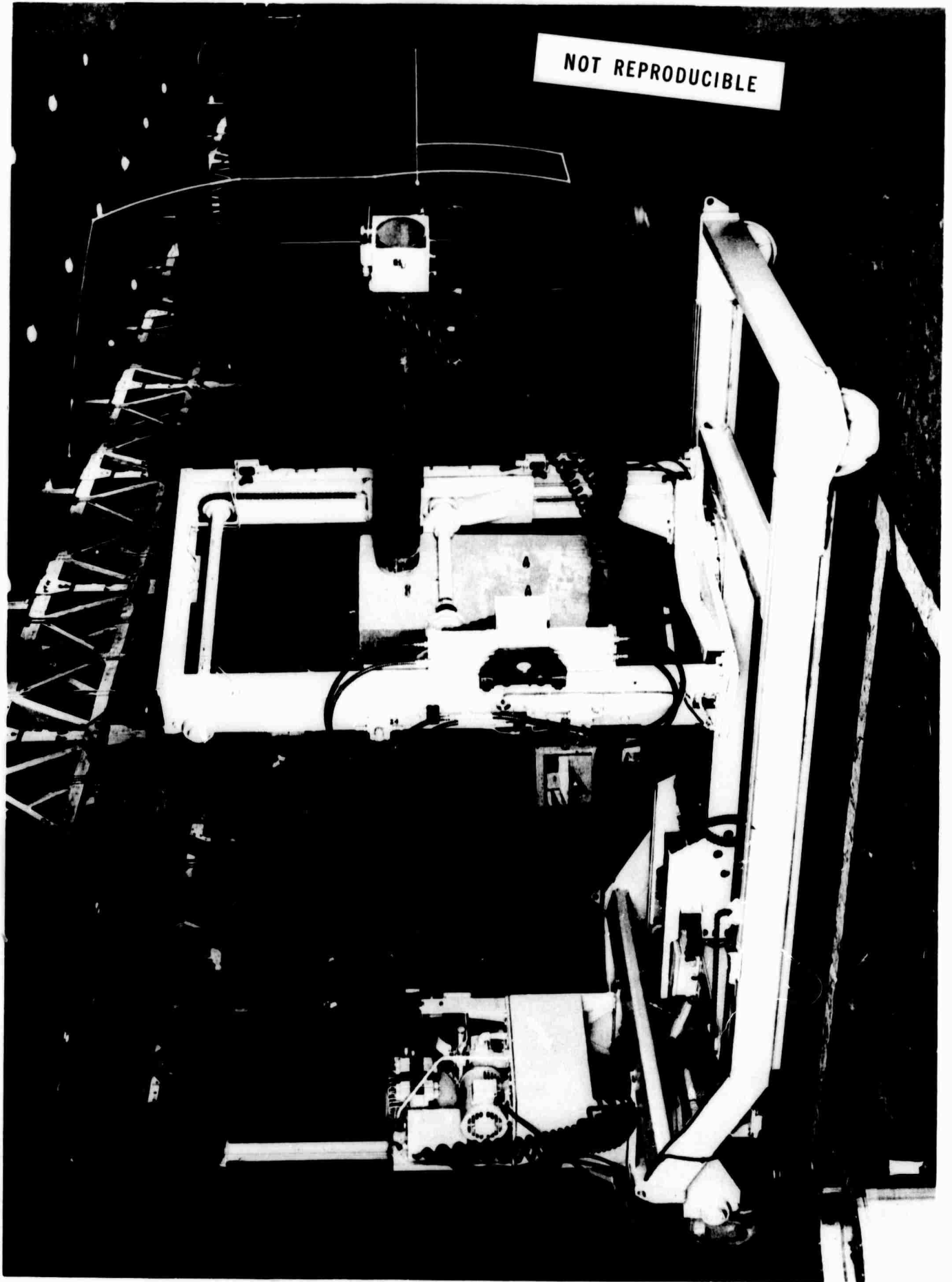


Figure 2-3. Time Exposure with Light Attached to End of Simulated Transfer Column During Translation

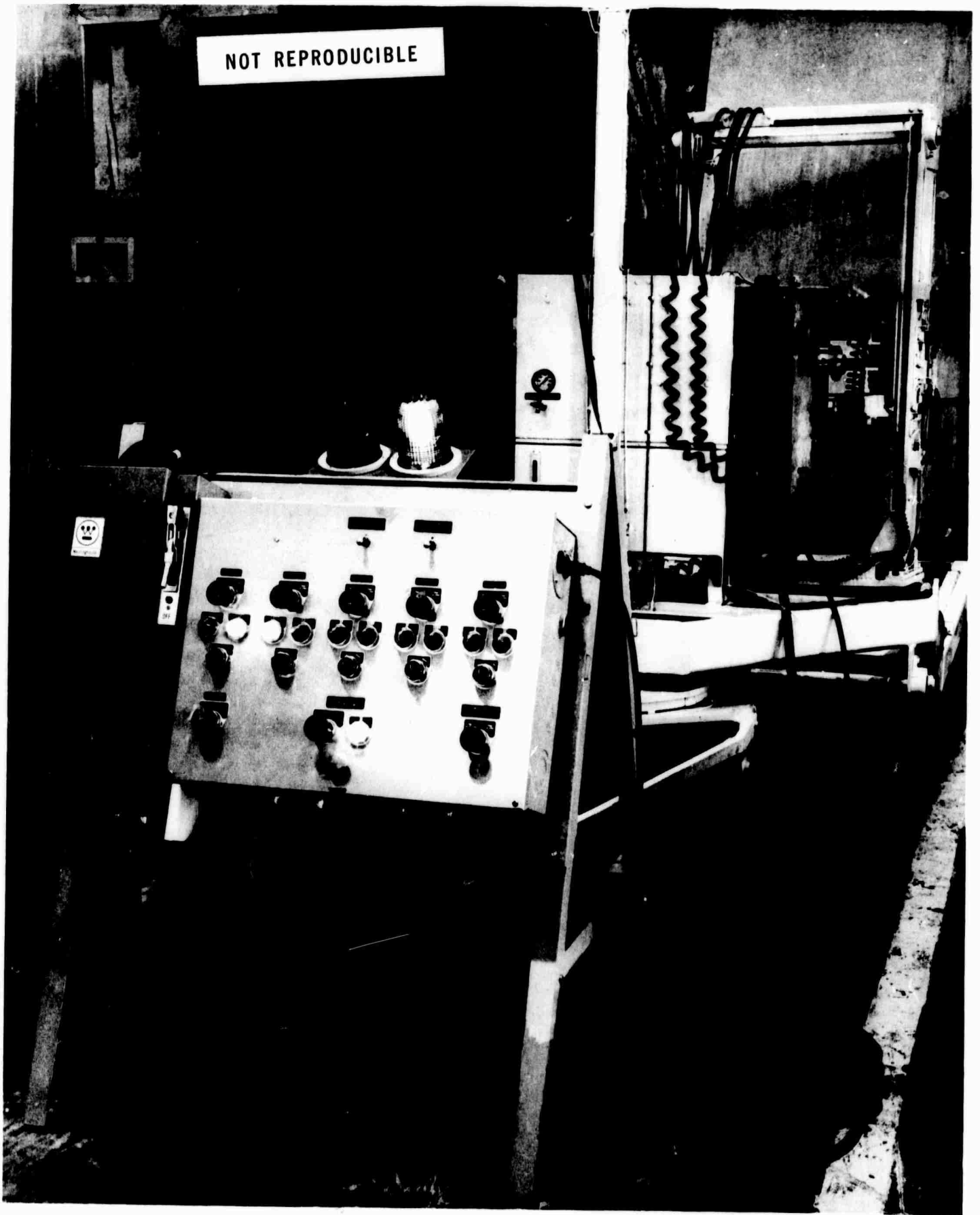


Figure 2-4. Control Panel for Electron Beam Gun Carriage

2.2.2 Modifications

In the preliminary testing, some discrepancies in carriage operation were noted. The clearances between the portions of the gun mount, which move in the Y-axis or vertical mode, were found to be excessive, and under certain loading conditions, the movable portions could be "derailed." A system of auxiliary guide rollers has been designed and installed to redistribute the loads, and thereby alleviate the problem. As mentioned in the First Quarterly Report (Ref. 3), a flexible coupling was provided in the gear drive system to prevent any misalignment problems that might result from a redundant center condition. Prior to its installation, the gear drive coupling was a rigid connection. The rigid coupling appeared to function properly but was removed anyway and replaced with the flexible device. The flexible rubber insert in the new coupling resulted in soft or spongy response in the yaw drive with a considerable amount of overshoot observed at the end of the actuator stroke and upon control valve closure. The rigid coupling will be reinstalled to eliminate these undesirable characteristics.

3. FIELD TESTS

3.1 TEST SITE SELECTION

Site review and selection have been conducted with considerations such as site geology, availability of support equipment and facilities, and location in mind. Toward the end of the first quarter of this contract, a tentative site selection was made after reviewing 12 quarry sites and an underground mine. The site selected was the Logan quartz gabbro quarry, a producer of crushed rock products, located near Watsonville, California. This site met most of the criteria for an acceptable site except the requirement for relatively unfractured rock. Since it is located on the San Andreas Fault, the Logan rock is extensively fractured and faulted. After a second visit to the Logan site by Westinghouse and Bureau of Mines personnel in June 1971, this site was rejected as a prime test site, and another site was located that more completely fulfills the desired geologic requirements.

The approved test site, also visited by Westinghouse and Bureau of Mines personnel, is the Raymond Granite Company's "Sierra White" granite quarry. The quarry is located in the Sierra Nevada foothills of California and 25 miles south-southwest of Yosemite National Park. A section of the USGS map for California gives an indication of geological formations in the Raymond area.**

The Raymond quarry is a producer of white granite dimension-stone products, which are excavated from an exposed face of an extensive mesozoic granitic formation. The rock is an even textured, fine grained moscovite-biotite granite, grayish white in color, and contains an extremely small amount

"Sierra White" is the producer's trade name for the rock from this quarry.

**See Mariposa Sheet of Olaf P. Jenkins' Edition of Geologic Map of California, Compilation by Rudolph G. Strand, U.S. Geological Survey, 1967.

of pyrites. The chemical composition of the rock and some of its physical properties are as follows:

Chemical Composition

Silica (SiO ₂)	73.92%
Alumina (Al ₂ O ₃)	14.90%
Ferric Oxide (Fe ₂ O ₃) and Ferrous Oxide (FeO) . . .	1.95%
Titania (TiO ₂)	0.14%
Manganese (MnO)	0.24%
Lime (CaO)	3.28%
Magnesia (MgO)	0.68%
Combined Water (H ₂ O)	0.32%
Soda (Na ₂ O) and Potash (K ₂ O)	4.51%
	100.00%

Physical Properties

Specific Gravity	2.64
Bulk Density (ASTM C97-47)	164.8 lb./ft. ³
Absorption (ASTM C97-47)	0.27%
Compressive Strength, Dry (ASTM C170-50)	34,800 psi
Compressive Strength, Wet (ASTM C170-50)	26,000 psi
Modulus of Rupture, Dry (ASTM C99-52)	2050 psi

In their excavation of the quarry, the operators have refrained from the use of explosives whenever possible, and therefore, the rock mass is almost entirely fracture-free.

While this site is ideal geologically, its use presents other difficulties, primarily because of its rather remote location. Utilities and telephone communications are available, but the closest living accommodations and medical facilities are in Madera. The support equipment and labor available

from the quarry operator is rather limited. He will provide a part-time electrician to provide power to the test face, but all other labor must be provided by Westinghouse. A small machine shop and some welding equipment are available for Westinghouse use, but again, personnel must be provided by Westinghouse.

3.2 SITE SUPPORT EQUIPMENT

Site support equipment includes the motor-generator sets for the EBG power supply, radiation detection and monitoring instrumentation, and radiation protection equipment.

3.2.1 Electron Beam Gun Power Supplies

Two portable engine-generator sets have been obtained for use in field test operations. A 100-kW, 208-volt, 400-Hz, 3-wire generator will be used for gun power and a 30-kW, 220-volt, 4-wire unit will provide power for the auxiliary equipment.

3.2.2 Radiation Studies

Wherever electrons are stopped by a target, x-rays are produced. This is the mechanism responsible for the production of x-rays used for medical and radiographic use and is also the source of radiation in television tubes. The stopping of electrons produces an x-ray flux with a continuous energy spectrum, starting at zero and reaching a maximum energy equal to that of the incoming electrons. (The short wavelength limit is given by $\lambda_{\min} = 12.4/E_0$, where E_0 is the electron energy in kilovolts. For the 36-kW electron beam gun, E_0 is 150 kV). Most of the x-ray flux has an energy of approximately two-thirds of this value, or 100 kV. In addition, characteristic x-rays of the target material are produced. This is monoenergetic "line radiation". The characteristic K-alpha line for tungsten has a wavelength of $\lambda_w = 0.209$ AU (corresponding energy is 60 kV). For uranium it would be $\lambda_u = 0.126$ AU (99 kV); for silicon, $\lambda_{si} = 7.111$ AU (1.75 kV). The composition of the target material can be determined by analysis of the produced x-ray spectrum.

Because of the complexity of the radiation situation, one cannot give a quantitative number for the x-ray flux produced and another for the amount of shielding required. To calculate the required shielding, one must assume a worst case and then through the use of empirically derived formulas, shielding requirements can be predicted.

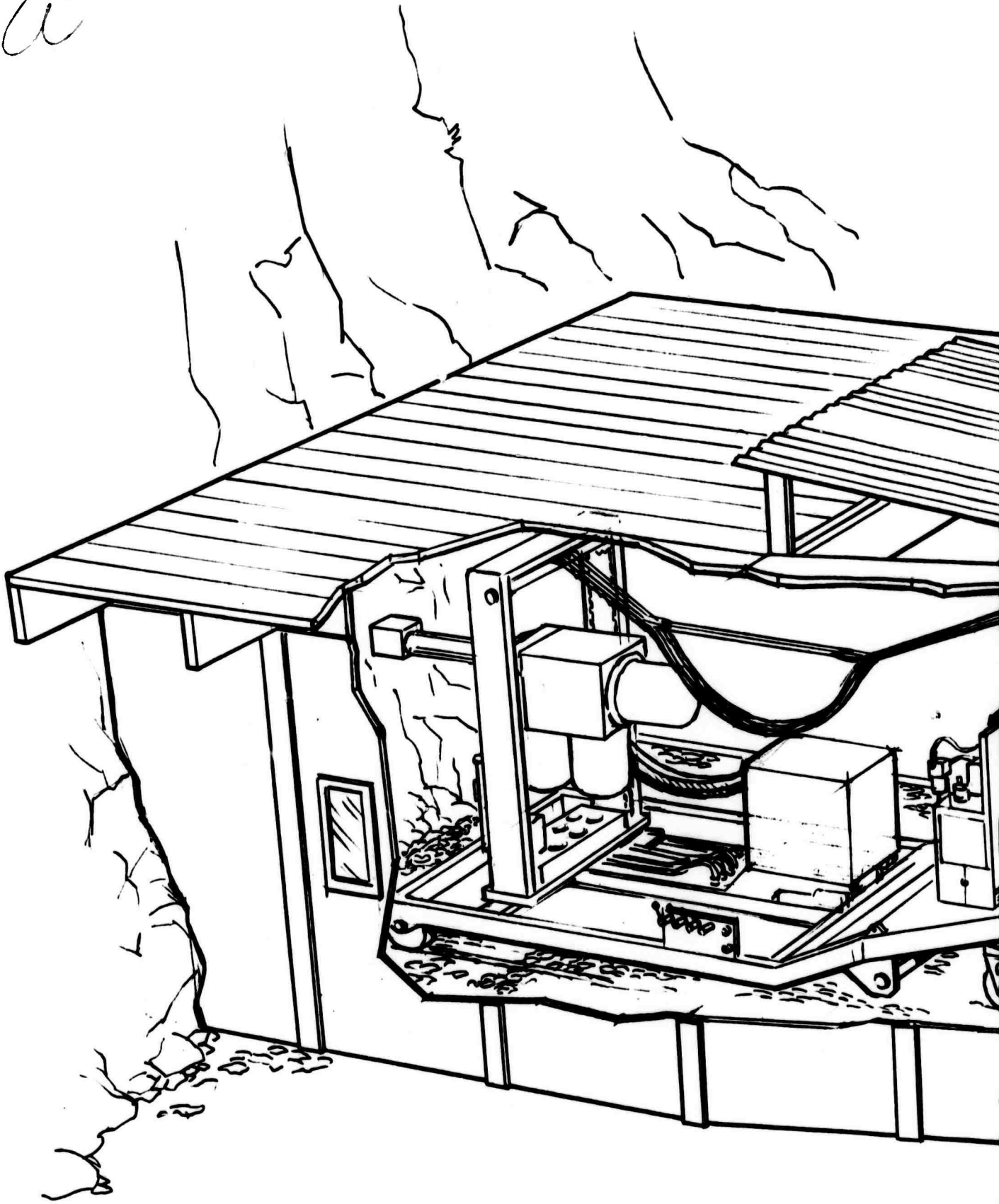
It should be noted that the assumed worst case results in a conservative shielding design, since the assumed radiation energy level exceeds the actual level by a significant amount. A certain amount of "self shielding" also occurs as the beam penetrates into the target material, but this "self shielding" was neglected in the prediction of shielding requirements.

3.2.2.1 Shield Design. The radiation intensity produced by a 150 kV, 36 kW beam impinging at a point of a flat surface of tungsten (atomic no. 74), according to standard formulas is 76,500 m² Roentgens per hour. The intensity from the point source falls off with the square of the distance (therefore the m² (square meter) term in the above units). The intensity is lower for targets of lower atomic number, in direct proportion to this number. For silicon (atomic no. 14), which is a major constituent of the target rock, the x-ray intensity is therefore 14,500 m² Roentgens per hour.

If the operator is located 2 meters from the source, the unshielded radiation flux would be 1/4 of the above number, namely, 3600 R/hour. This is the flux for which shielding will be designed. A lead shield gives the best shielding effect per unit weight for the x-ray energy range in which we are working.

A concept design for field test site radiation shielding has been developed, based on these intensity calculations. The radiation shield design consists of a plywood shed 16 feet wide by about 24 feet long by 8 feet high. The walls are lined with 1/4-inch lead in the areas closest to the radiation source and with 3/16-inch thick lead in areas further removed from the source. The rear wall of the shield structure is a free-standing baffle, which may be removed with a small crane to permit removal of the gun and support carriage without disassembly of the structure. Three leaded glass windows are provided for observers and operators. The roof of the shed is partially covered with heavy structural timber and a thin lead sheet, which offer protection from falling rock and also reduce the intensity of air scatter or "sky shine" radiation to permissible levels. An artist's concept of the shield structure appears in Figure 3-1.

a



B

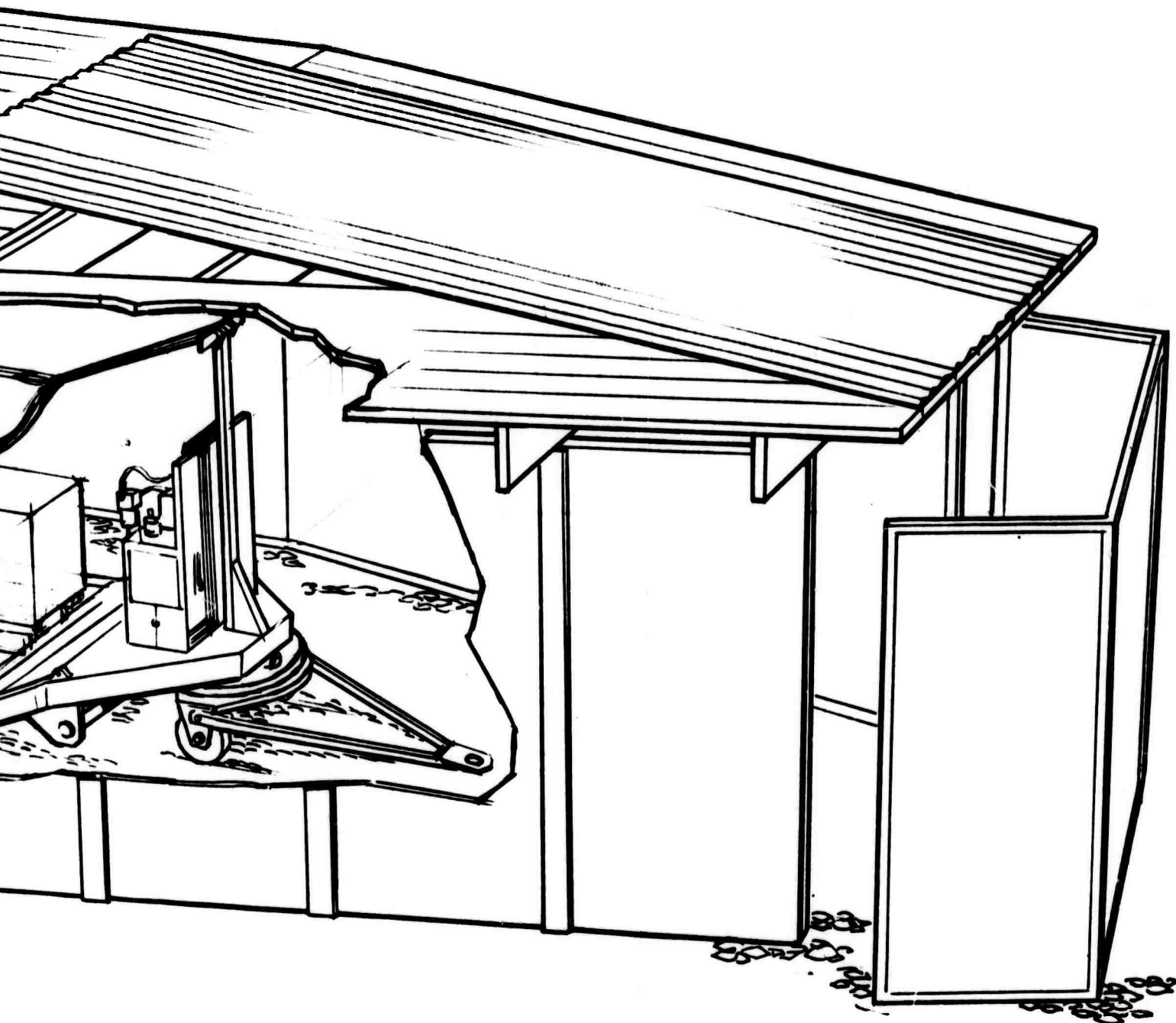


Figure 3-1. Artist's Concept of Test Site Shield Structure

3.2.2.2 Monitoring and Detection Equipment. During these initial field tests, extensive radiation intensity measurements will be made: (a) to accumulate more data about the amount of x-rays actually produced with a particular rock target, and (b) to give absolute assurance of the operators' safety. Ionization chamber type of radiation meters (calibrated in 'Roentgens per unit time' for all wavelength of x-rays) will be used, as well as pocket dosimeters and film badges. The gun control is also equipped with an audible/visual Gamma alarm, which is interlocked to the beam in the event of high exposure rates. (Radiation safety codes require the use of film badges in any radiation area where the dose rate may exceed 2 milliroentgens per hour.)

4. THEORETICAL STUDIES

4.1 PIERCING WITH ELECTRON BEAM

The piercing process was fully described in the First Quarterly Report (Ref. 3, p. 5-2). The following discussion extends the previous work, except that a different scheme is used for the computations of the temperature distribution in the rock. The new calculations are based on a model which will better approximate the fact that, at the base of the piercing cavity, the melt-front moves much faster than any "heat wave."

4.2 DEVELOPMENT OF THERMAL STRESSES WITH TIME

Experience gained during the previous quarter concerning the rate at which electron beams penetrate rock has been applied to the calculation of the resulting thermal stresses. These stresses, in turn, cause the rock to crack. To allow for eventual correlation of the results with experimental data from a 9-kW gun, the calculations assume an EBG that delivers 9 kW at 150 kV and is 1/2 inch from the rock face. The size of the rock is typical of a laboratory sample. It is a cylinder, 10 inches in radius and 10 inches high. The beam pierces the center of one of the circular ends. This gives convenient boundary conditions for the existing computer programs.

The calculations are meant to clarify the mechanisms by which the electron beam causes rock to fail. The type of rock used for the calculation is fictitious. The cavity growth under an electron beam is assumed to be similar to that of Oklahoma gabbro (Ref. 3, p. 5-2); the elastic parameters, similar to those of Dresser basalt (Ref. 4); and the melting temperature, that of silica, i.e., 1700° C (Ref. 5).

To provide the desired information on the time development of the thermal stresses, six separate stress calculations were made; all conditions were the same except that each successive calculation was made for a longer piercing time. The six elapsed times were 5, 10, 20, 40, 80, and 300 seconds.

4.3 CAVITY MODEL

As mentioned in the First Quarterly Report, the simple approximation chosen as a model for the typical cavity consists of a cylindrical hole with a hemispherical base. The cavity depth d is given as a function of time t by the equation (Ref. 3, p. 4-6),

$$d = \left\{ \frac{4W_0}{2 \pi \alpha H^*} t + z_0^4 \right\}^{1/4} - z_0 \quad (1)$$

where W_0 is the electron beam power; H^* , the heat of "removal" (partly melting, partly vaporization, see Figure 5-3 of Ref. 1) of the rock; α , a parameter characterizing the spread of the beam due to multiple scattering; and z_0 , the distance from the original rock face to the point inside the electron gun where the beam begins to scatter. Table 4-1 gives the values of these parameters chosen for the present calculation for the 9-kW, 150-kV gun.

Table 4-1

PARAMETER VALUES FOR DEPTH VS. TIME FUNCTION
(9-kW, 150-kV ELECTRON BEAM GUN)

<u>Parameter</u>	<u>Value</u>
W_0	9.0 kW
H^*	223 kJ/in ³
α	$2.78 \times 10^{-3} \text{ in}^{-1}$
z_0	0.941 in

The radius of the hole is taken as its depth divided by 8.4, a value determined experimentally to be typical of several types of rock (Ref. 3, p. 5-12).

4.4 TEMPERATURE DISTRIBUTION

To avoid lengthy and costly computations required to solve the time-dependent heat flow equation with complicated boundary conditions, the following simplifying assumptions are made for temperature-distribution calculations:

1. The radius of the cylindrical cavity remains constant while its length grows.
2. The thermal diffusivity is constant with temperature and independent of direction. The value chosen as typical is 8×10^{-4} in²/sec (Ref. 6).
3. The radial temperature distribution in any one plane perpendicular to the z-axis can be calculated using the solution to the time-dependent heat equation appropriate for an infinitely-long, hot cylinder of constant temperature, T_m , imbedded in an infinite medium at an initial temperature of zero (Ref. 3, p. 4-9). The solution is a function of the radius of the cylinder, the radial coordinate of the point of evaluation, the elapsed time, and the thermal diffusivity.
4. The elapsed time used in evaluating the temperature distribution at any plane z in the rock depends on the depth z of the plane, since heating time is longest at the surface of the rock (z=0) and drops to zero at the depth of the hole (z=d) and beyond. Specifically, the heating time is the difference between the piercing time needed to reach the full depth, at which the beam is shut off, and the piercing time needed to reach the depth z of the point of evaluation. Using equation (1) yields

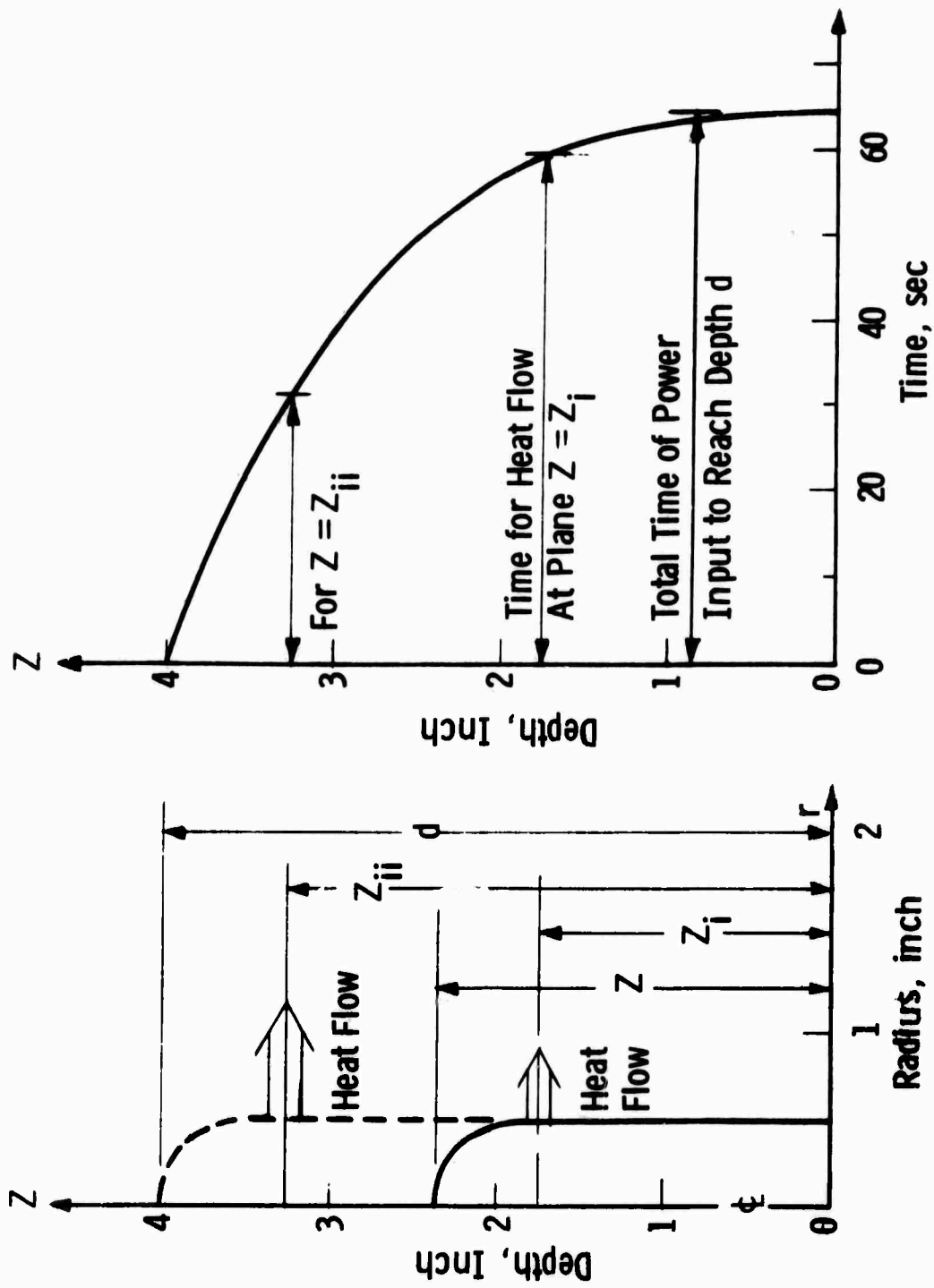
$$t_{\text{heating}}(z) = \frac{2 \pi \alpha H^2}{4w_0} \left\{ (d+z_0)^4 - (z+z_0)^4 \right\}$$

Figure 4-1 shows this time during which heat flow takes place in any plane perpendicular to the z-axis at depth z, as though a "snap-shot" picture were taken at the moment when the cavity attains a depth of 4 inches. In this and the following figures, the cavity "depth" z is going upwards, because the computer printouts were oriented and legible in this position.

5. The value of the cylinder radius used in the temperature function at depth z is taken to be the radius of the circle produced when the plane defined by z cuts the cavity. In most cases, therefore, the appropriate radius is simply the radius of the cylindrical portion of the cavity. However, at values of z approaching the depth of the cavity, the radius becomes that of the circle formed by passing the plane through the spherical bottom of the cavity, and this radius was used in the calculations.

Figures 4.2(a) through 4.2(f) show isotherms plotted using the above model. The cavity boundary is assumed to remain at 1700° C; the isotherms are shown in increments of 100° C. Each figure represents one of the six piercing times considered in the study. Notice that the isotherms converge to a point at the bottom of the hole. In this way, the model approximates the very steep temperature gradient at that point, which results from the advancing motion of the melt front. This appears to be a better approximation of the real temperature distribution than the previously used model shown in Figure 4-2 of Ref. 1. The cavity depth increases much faster than the heat can diffuse into the rock. The extent of this effect can be estimated by assuming for the moment that the speed of penetration is constant. With this simplification, an upper limit can be calculated for the small distance that heat will penetrate into the rock at the bottom of the hole. The temperature rise at a distance Δz below the bottom of the hole will be given by (see Ref. 7),

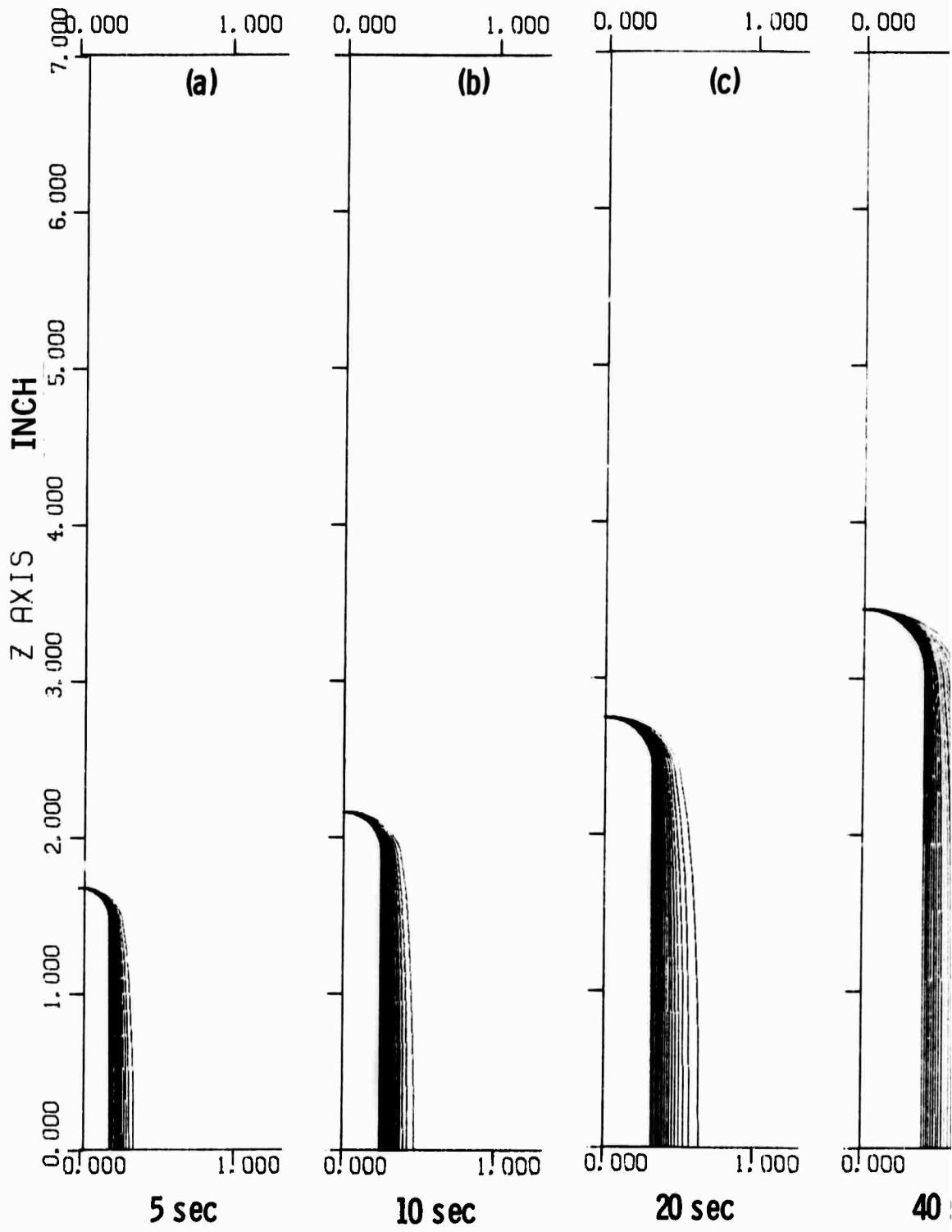
$$T = T_m \exp \left[- \frac{V \Delta z}{D} \right] \quad (2)$$



Assumed Shape of Cavity **Time for Radial Heat Flow**

Figure 4-1. Time for which Heat Flow Takes Place in Any Plane Perpendicular to Z-axis

a



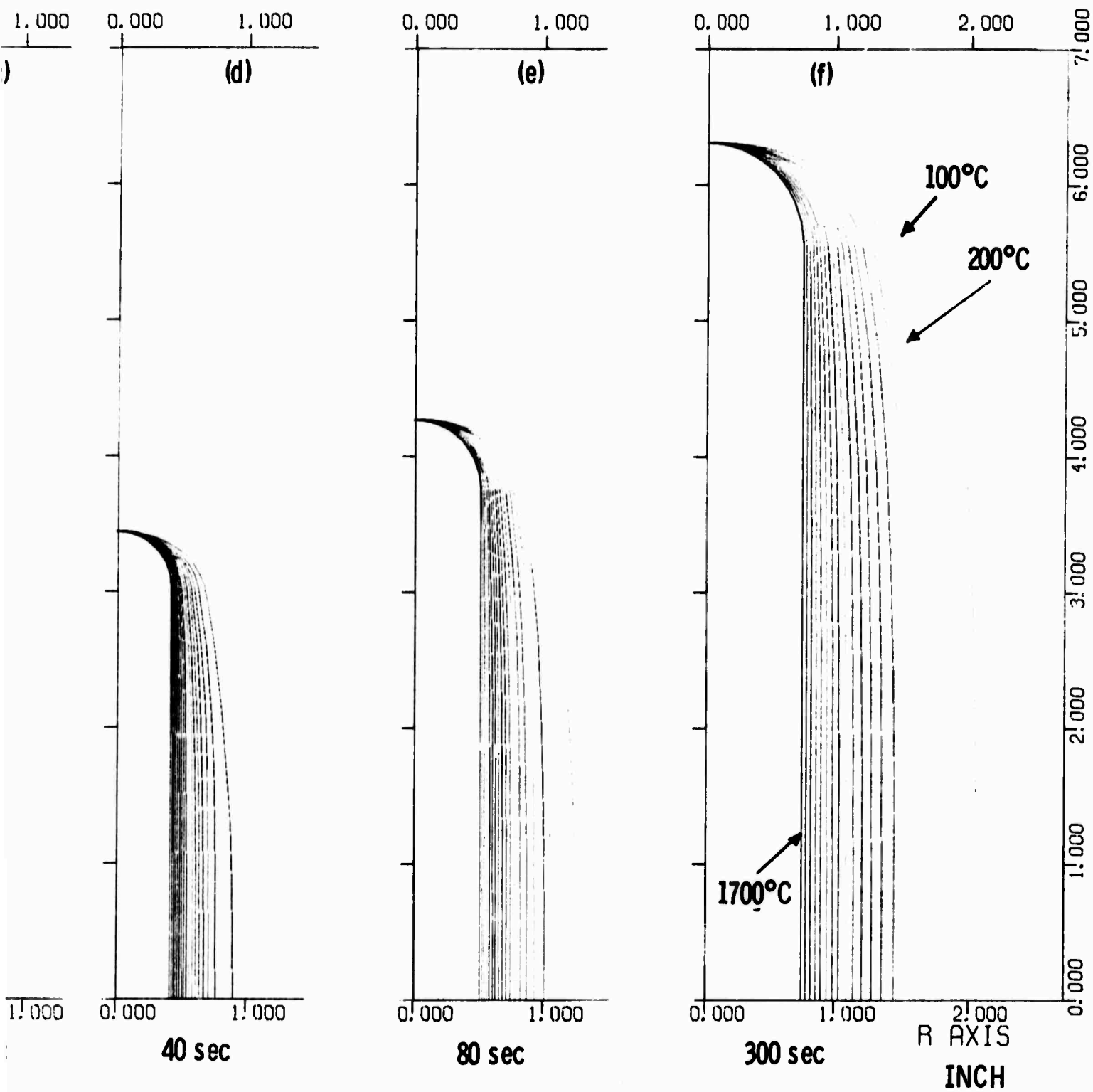


Figure 4-2. Calculated Isotherms Using Simple Model with Cavity Boundary at 1700°C

where T_m is the melting temperature of the rock (the temperature of the cavity wall); V , the speed that the melt front is advancing (assumed here to be constant); and D , the thermal diffusivity. For V , the formula in Ref. 3, p. 4-6 is used to give

$$V = \frac{W_0}{H \cdot 2 \pi \alpha (d+z_0)^3} \quad (3)$$

which gives the penetration speed of the electron beam for a given depth d . (The parameters in equation (3) are the same as those of equation (1)). Combining equations (1), (2), and (3) gives

$$\Delta z = \frac{H \cdot 2 \pi \alpha}{W_0} \left\{ \frac{4W_0}{2 \pi \alpha H} t + z_0 \right\}^{3/4} D \ln \frac{T_m}{T} \quad (4)$$

Figure 4-3 shows plots of equation (4) giving the distance of penetration of temperature into rock below the end of the cavity as a function of piercing time for several values of temperature under the conditions listed in Table 4-1 with $D = 8 \times 10^{-4}$ in²/sec and $T_m = 1700^\circ$ C. The arrows in Figure 4-3 designate the times chosen for the stress calculations. As one would expect, penetration of the heat into the solid rock increases with time and for lower temperatures. Contrary to the simplifying assumption made in the above calculation, the speed V is not a constant but is, in fact, a decreasing function of time. Accordingly, the actual heat penetration rates at the base of the cavity will be even slower than those given by equation (4).

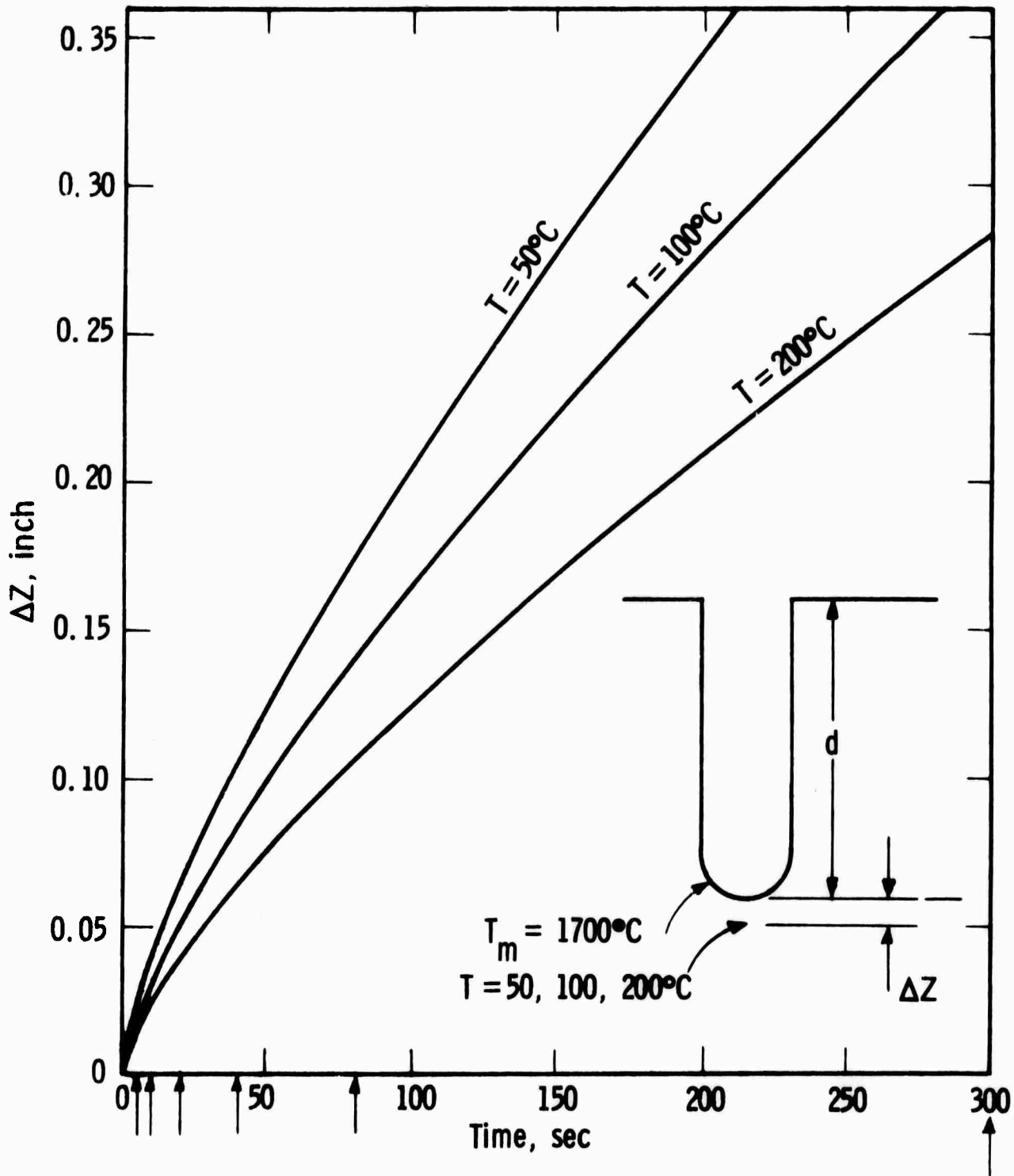


Figure 4-3. Distance of Temperature Penetration into Rock Below End of Cavity as Function of Piercing Time

4.5 THERMAL STRESS CALCULATIONS

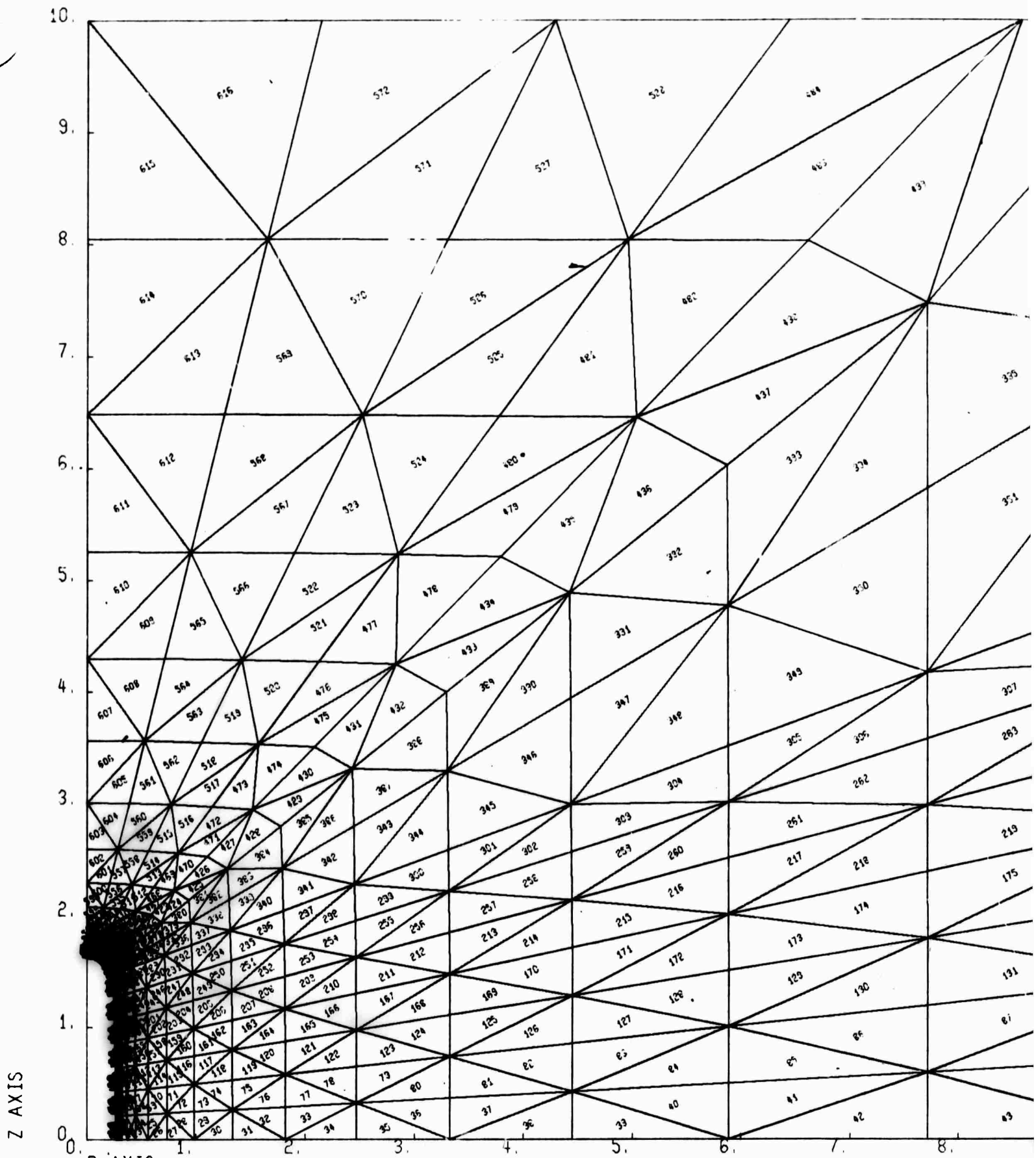
Thermal stresses in the rock were calculated using a package of finite-element computer programs whose details are proprietary. Another program, TEMPMAT, was used to prepare the additional input data temperature field, etc. for the stress calculations.

Meshes for two of the runs, No. 2.1 (5 seconds - the shortest time) and No. 2.6 (300 seconds - the longest time) are shown in Figure 4-4. Note that the nodal points are spaced closely together in the general direction of the temperature gradient and are kept rather close together in the region of greatest interest, i.e., just outside the heated region where the highest tensile stresses are expected. Instead of starting at the walls of the cavity, the mesh begins on the 700° C isotherm, which is taken as the temperature at which the rock becomes plastic.

The program TEMPMAT calculates the temperature for each mesh nodal point and punches out the values, which are then used as inputs for the stress calculation programs. In addition, to approximate the variations with temperature of the elastic and thermal properties of the rock, TEMPMAT makes use of a material type-specification in the stress calculation programs and assigns to each element a value for each of the elastic and thermal parameters according to the average temperature of the element (see Table 4-2).

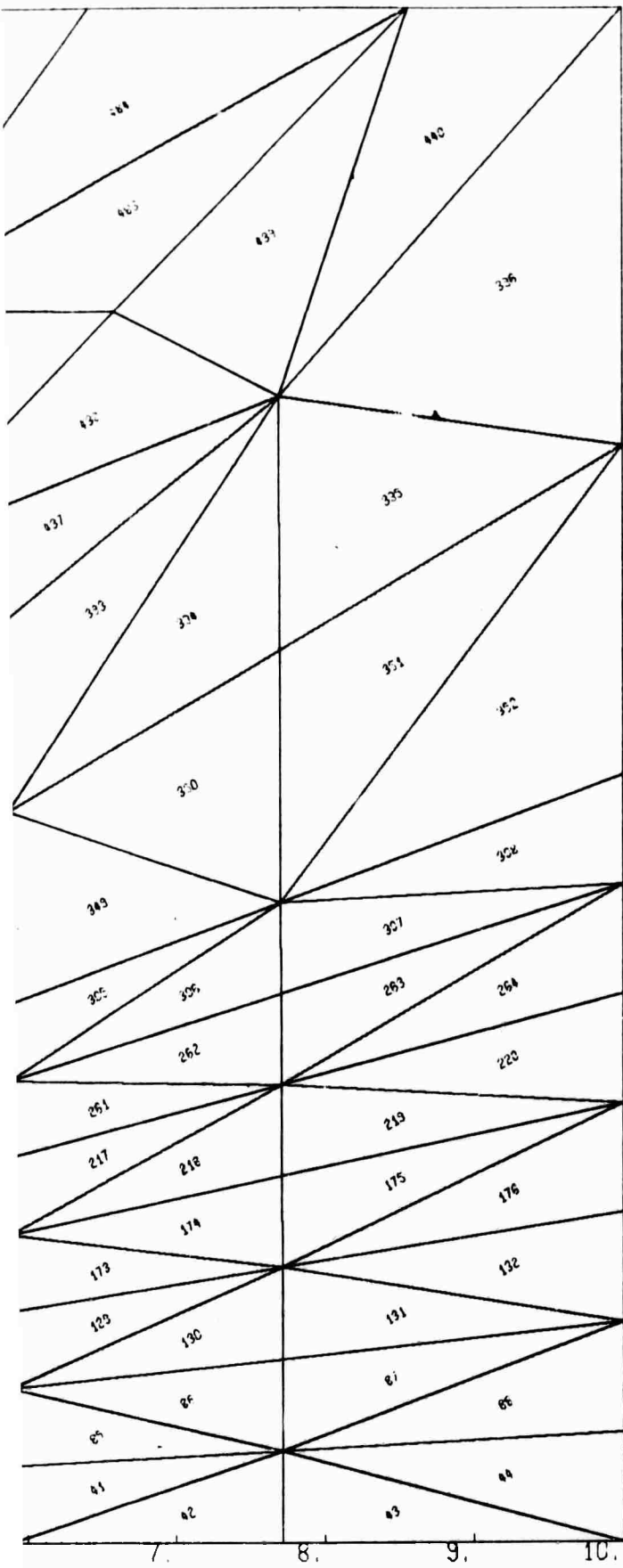
Figures 4-5 through 4-8 show the results of the stress calculations. Four different stresses are shown: (1) azimuthal tension (θ stress), (2) maximum (tensile) principal stress in the r-z plane, (3) azimuthal compression, and (4) minimum (compressive) principal stress in the r-z plane.

a



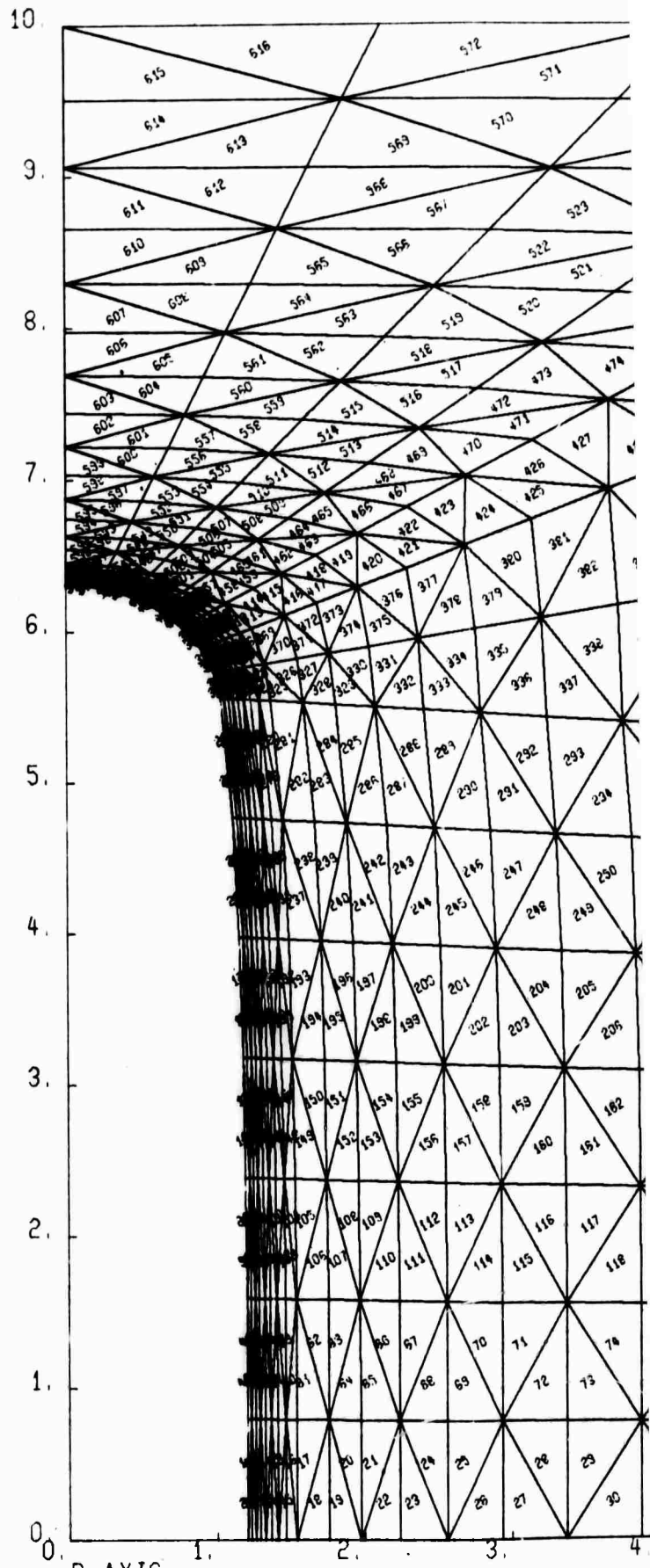
R AXIS
RUN2.1 5 SEC 9 KW CYLINDRICAL BLOCK OF ROCK 20IN DIA X 10IN HIGH ELEMENT GEOMETRY

(a)

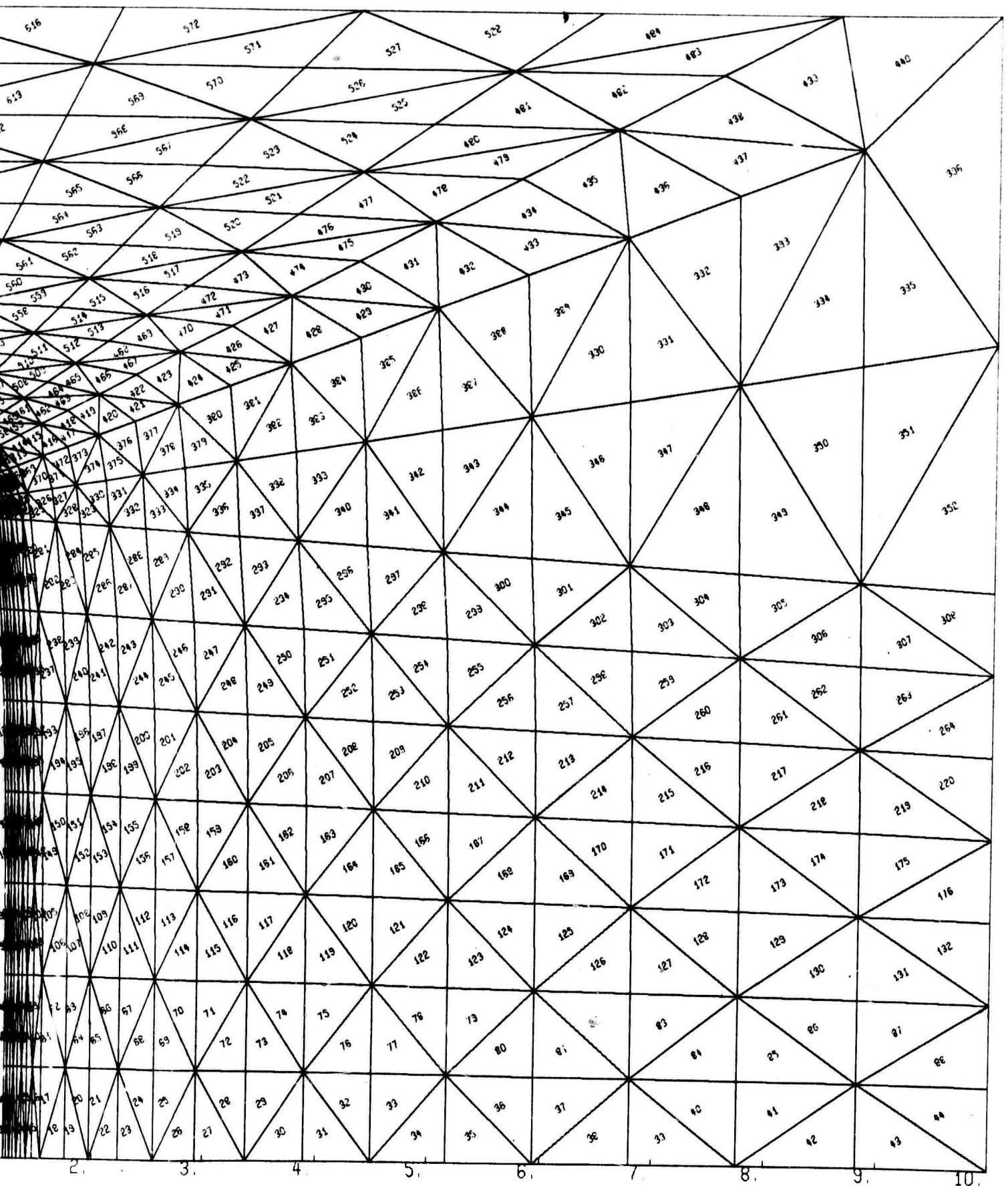


JOIN HIGH ELEMENT GEOMETRY

13



R AXIS RUN2.6 300 SFC 9 KW CYLINDRICAL BLOCK

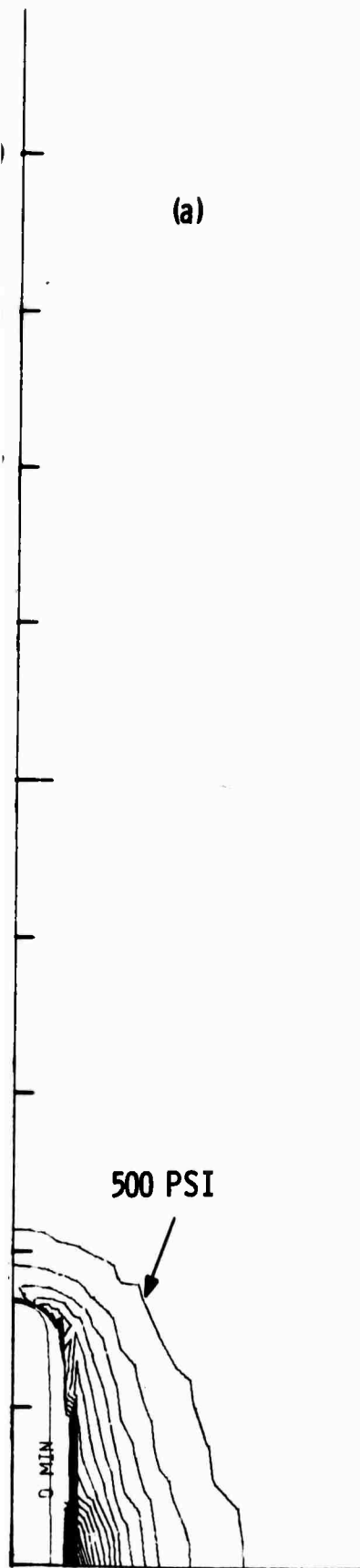


FC 9 KW CYLINDRICAL BLOCK OF ROCK 20IN DIA X 10IN HIGH ELEMENT GEOMETRY

(b)

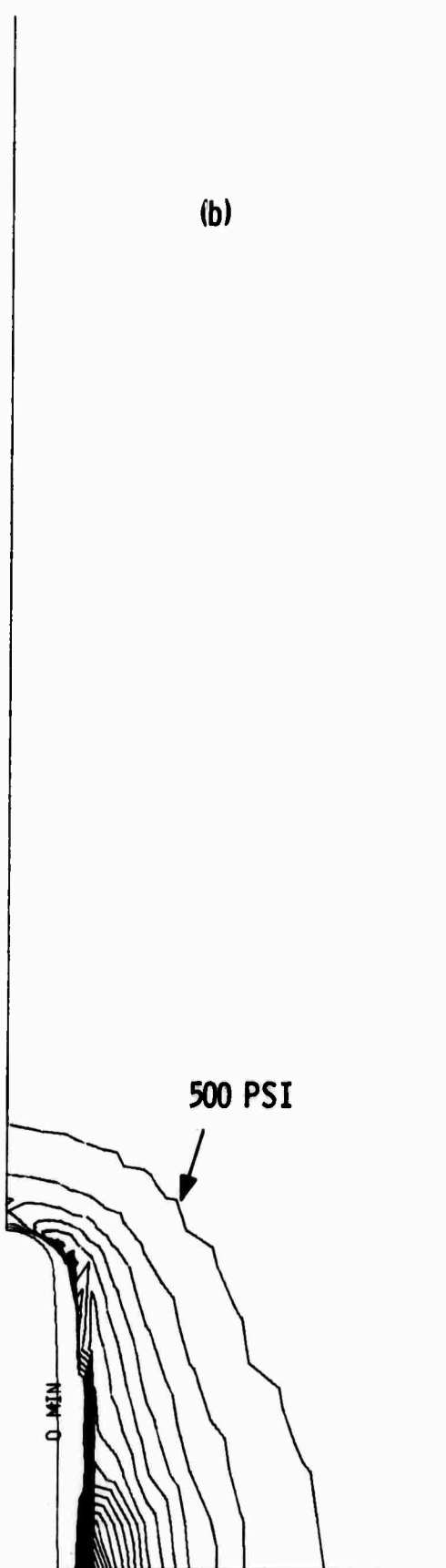
Figure 4-4. Finite Element Triangular Meshes:
 (a) Computer Run 2.1 (5 seconds)
 (b) Computer Run 2.6 (300 seconds)

(a)



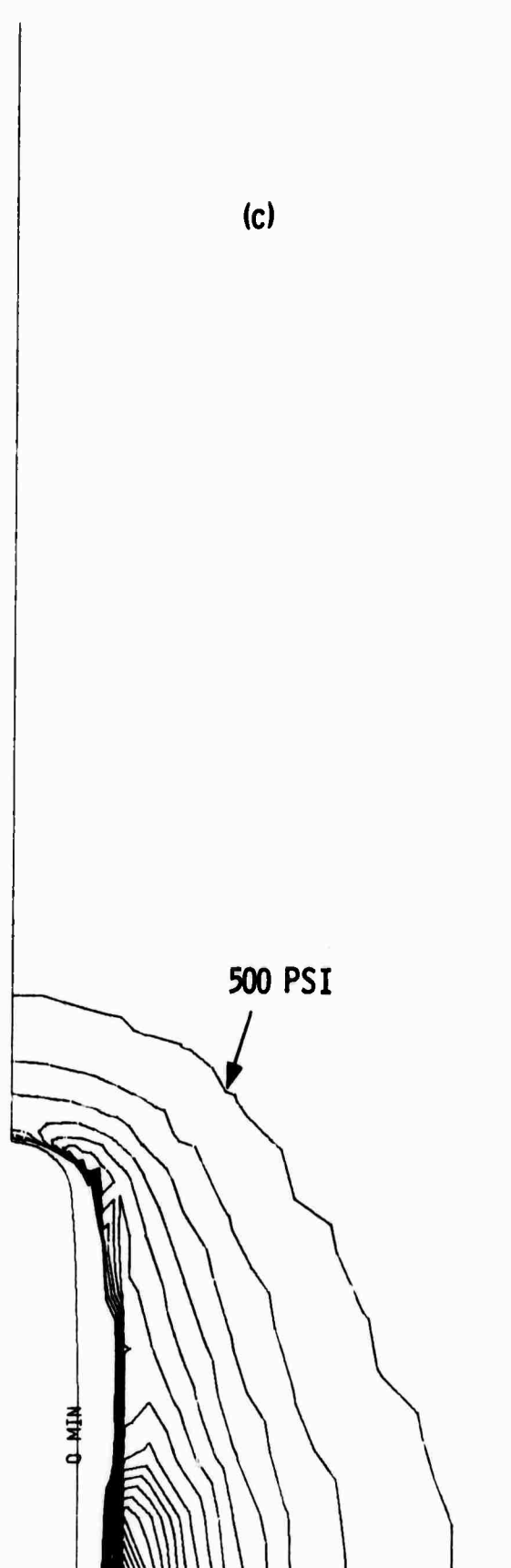
R AXIS
RUN2.1 5 SEC

(b)



R AXIS
RUN2.2 10 SEC

(c)

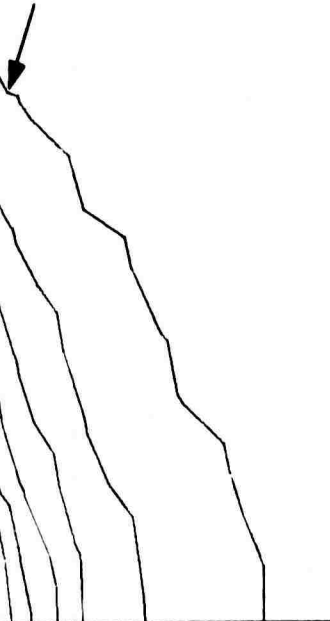


R AXIS
RUN2.3 20 SEC

a

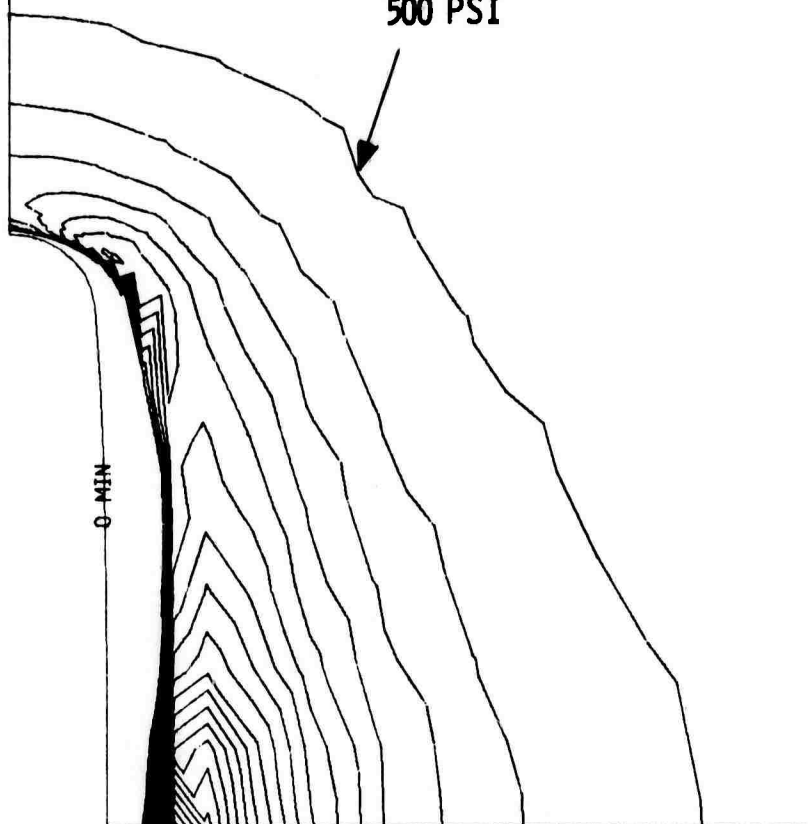
(c)

500 PSI



(d)

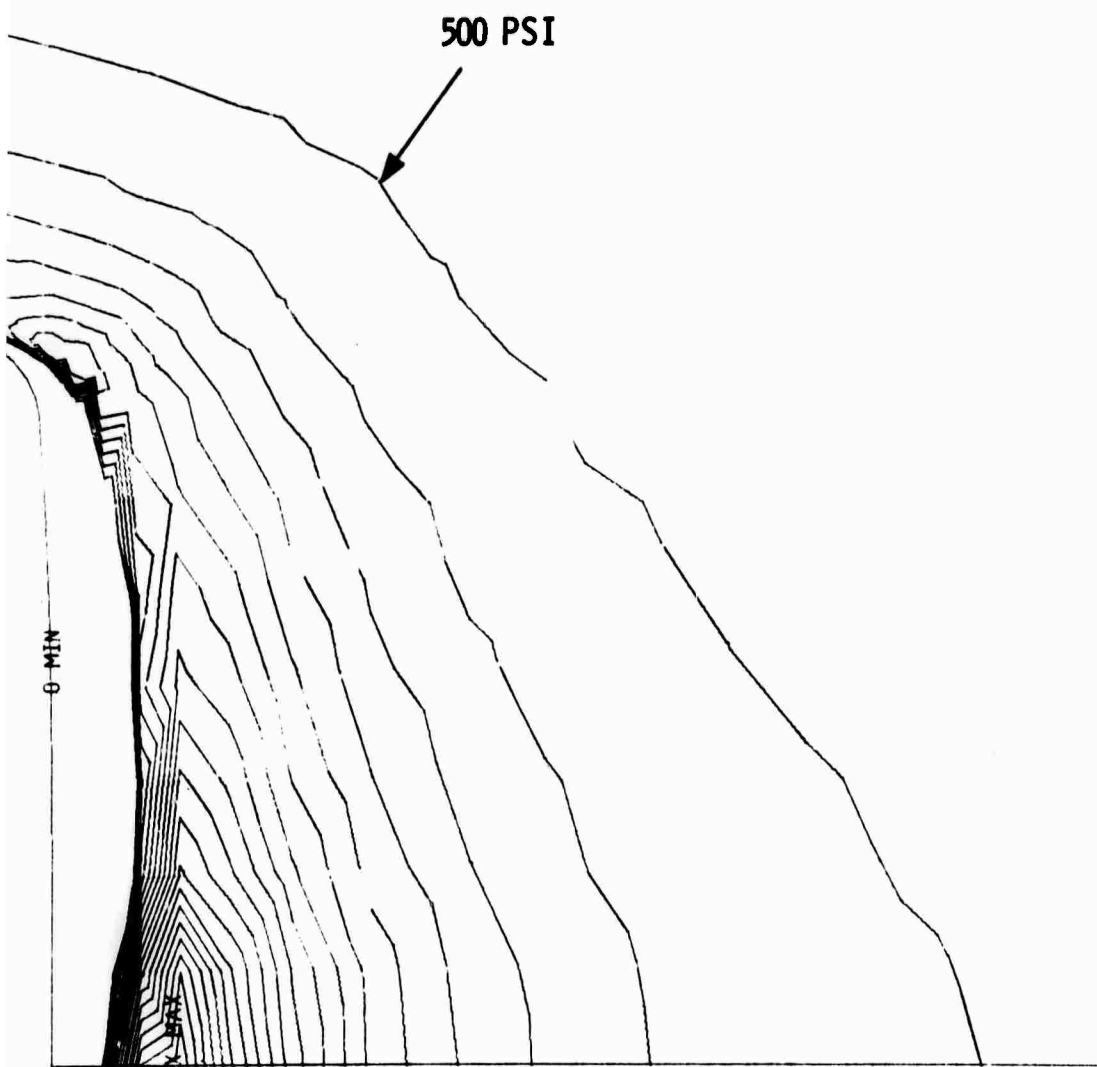
500 PSI



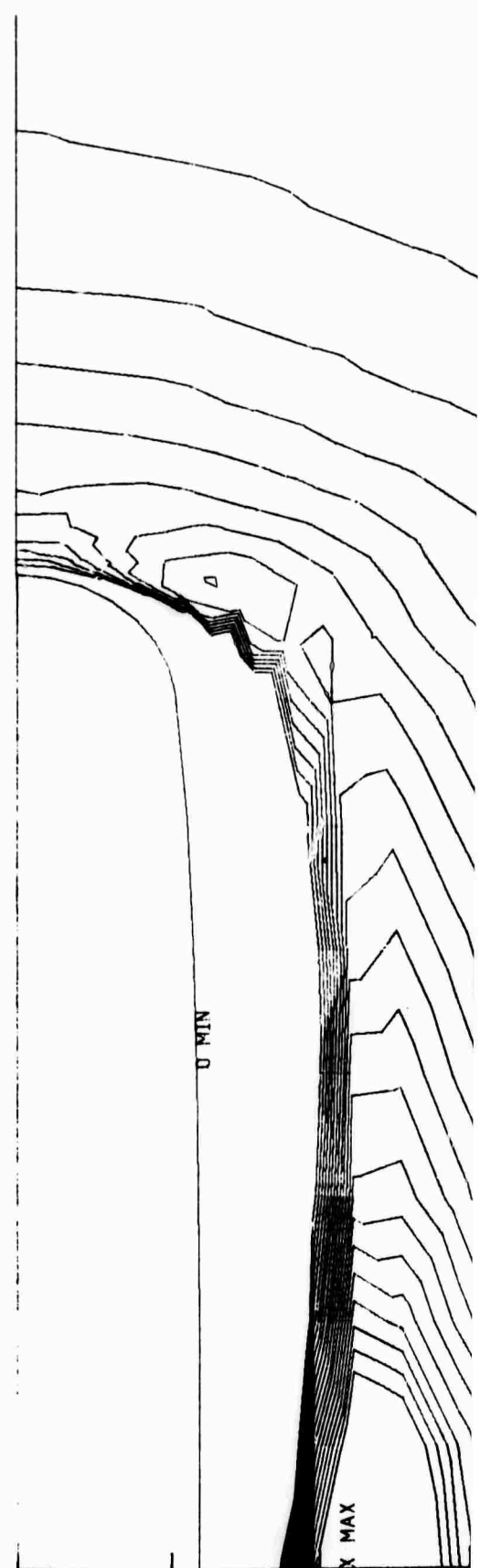
R AXIS
RUN2.4 40 SEC

R AXIS
RUN2.5 80 SEC 9 KW

B

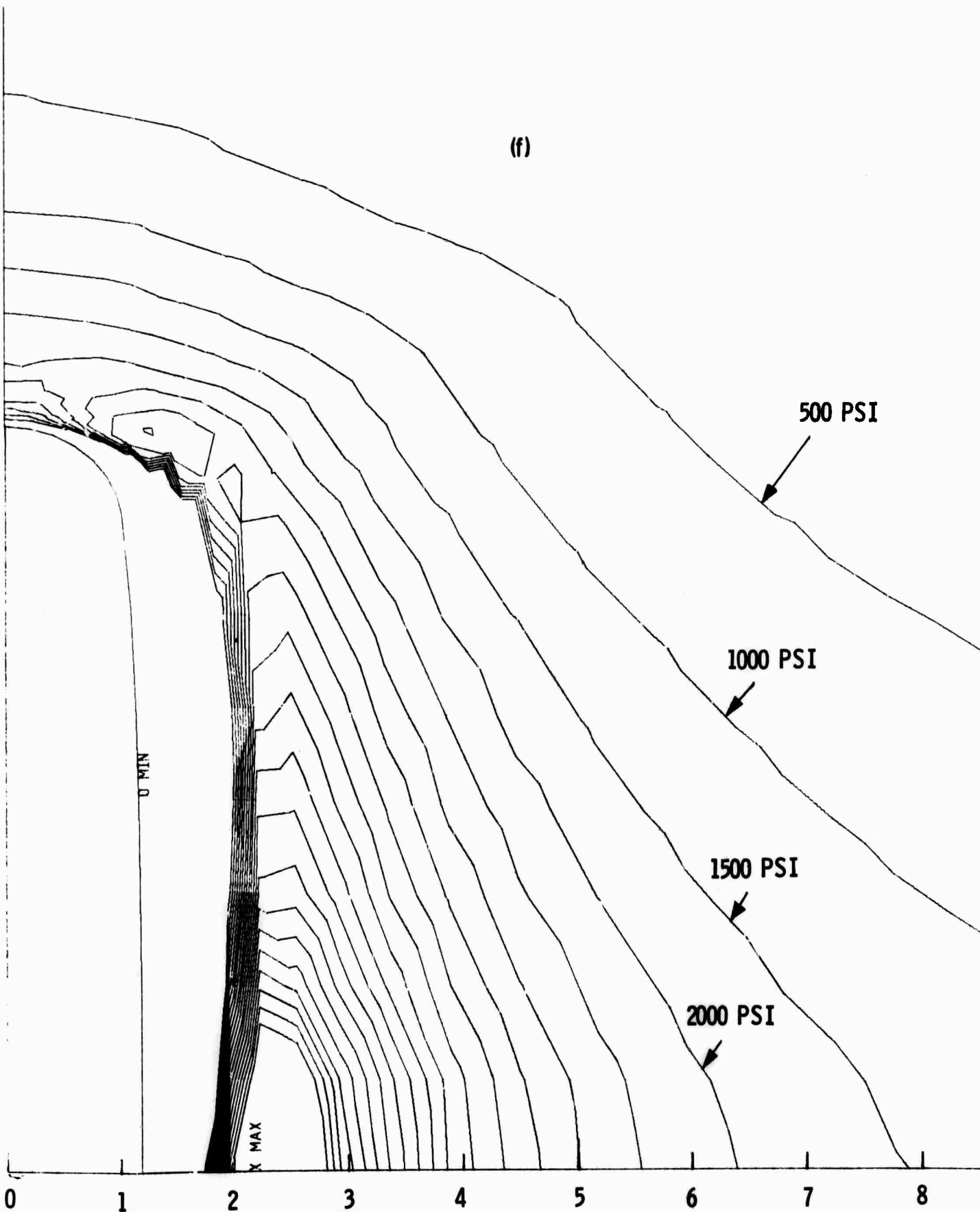


IS 5 80 SEC 9 KW CYLINDRICAL BLOCK OF ROCK 20IN DIA X 10IN HIGH



0 1 2 3
R AXIS INCH
RUN 2.6 300 SEC 9 KW CYLIN

C

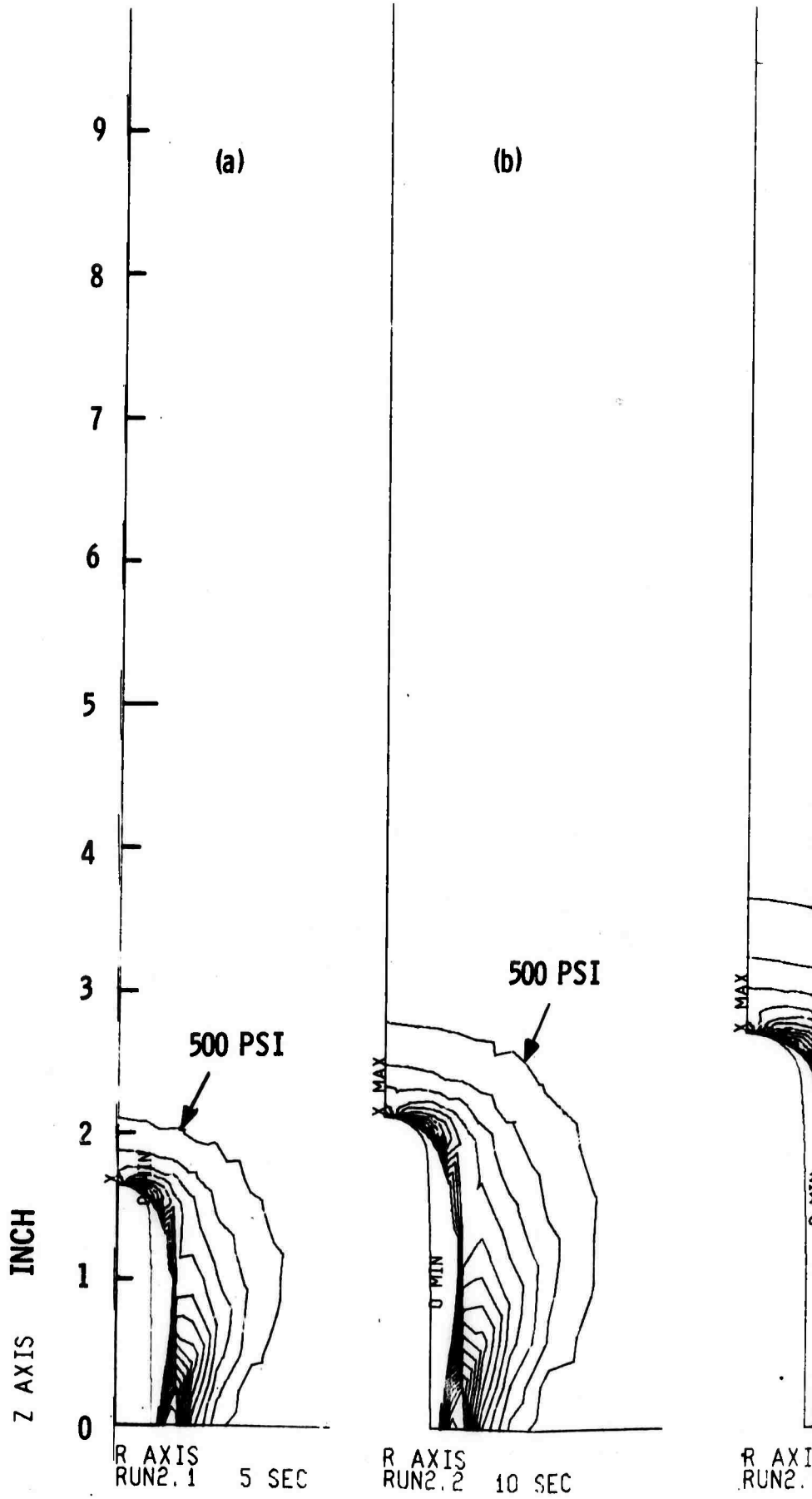


IGH

R AXIS INCH
 RUN 2.6 300 SEC 9 KW CYLINDRICAL BLOCK OF ROCK 20IN DIA X 10IN HIGH θ STRESS

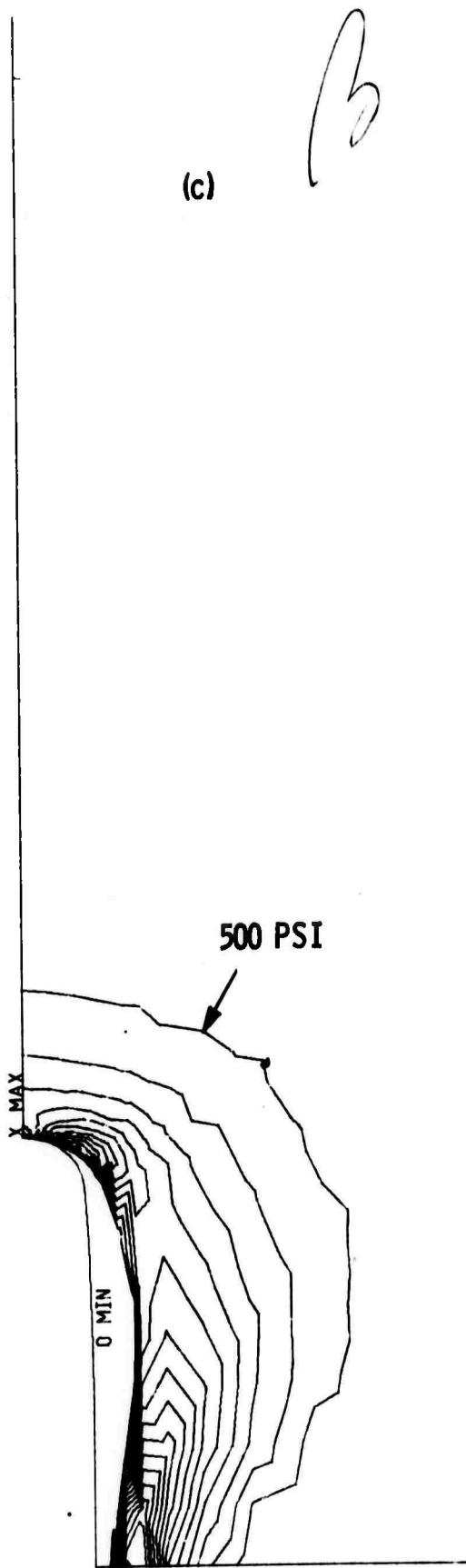
Figure 4-5. Calculated Azimuthal Tension (θ Stress) for Piercing Times of 5, 10, 20, 40, 80, and 300 Seconds

2

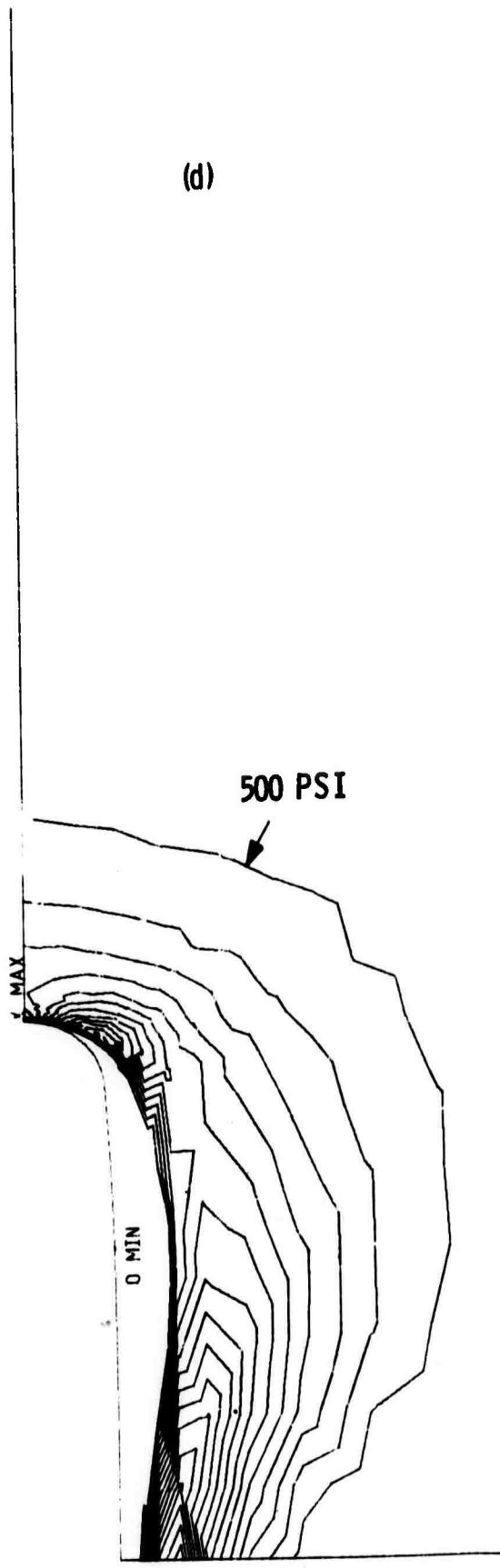


0 PSI

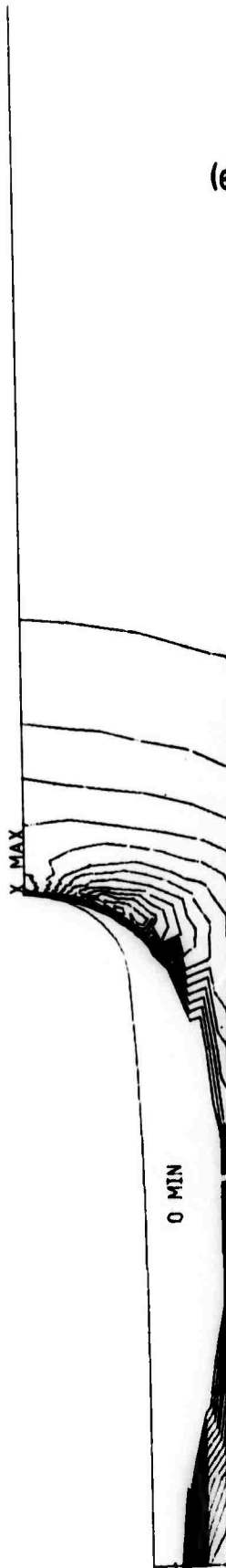
SEC



R AXIS
RUN2.3 20 SEC

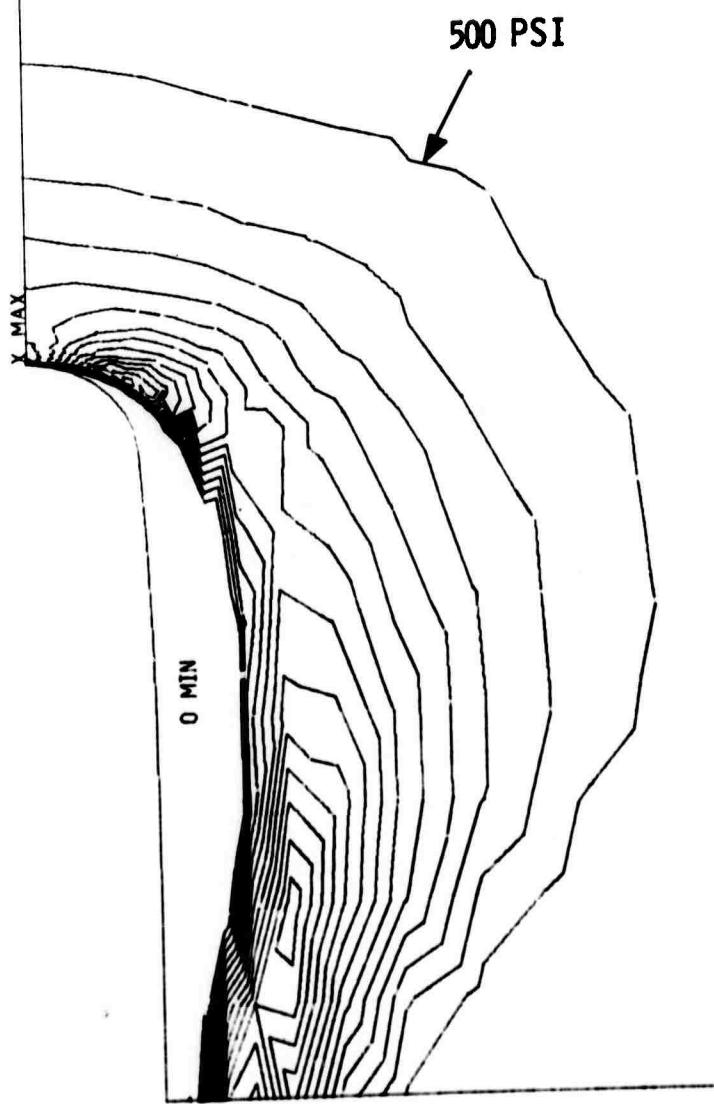


R AXIS
RUN2.4 40 SEC



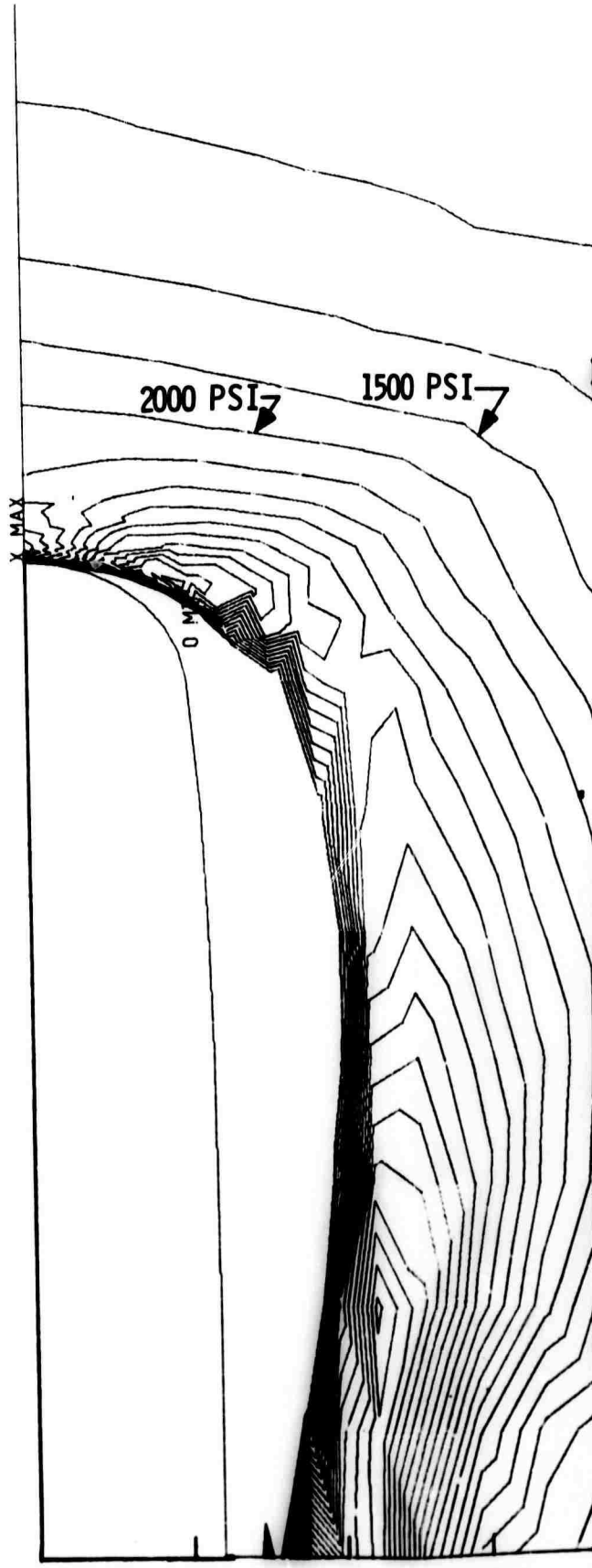
R AXIS
RUN2.5 80 SEC

(e)



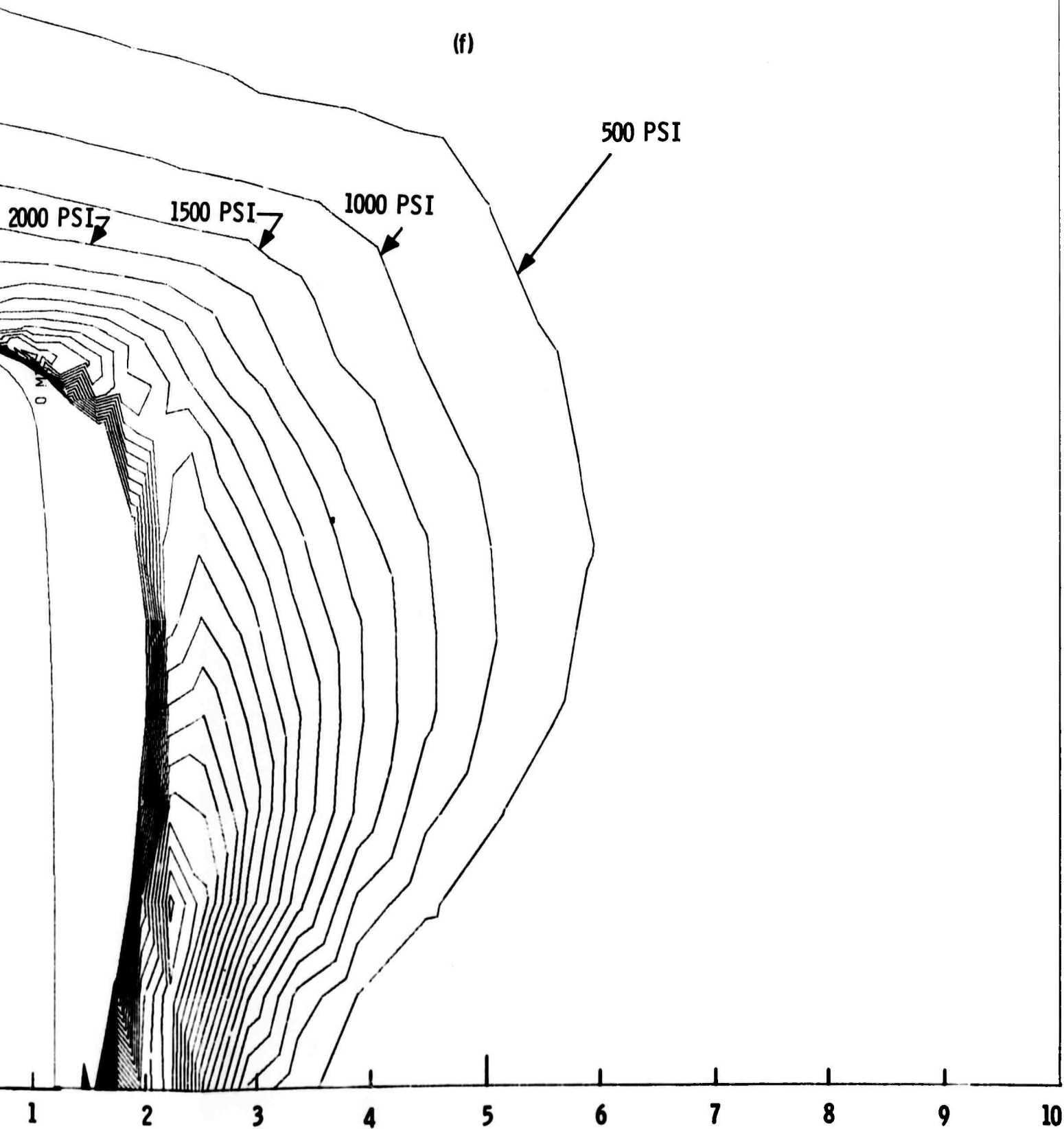
R AXIS
RUN2.5 80 SEC

C



0 1 2 3

R AXIS INCH
RUN2.6 300 SEC 9 KW CY



(f)

500 PSI

1000 PSI

1500 PSI

2000 PSI

0 PSI

1 2 3 4 5 6 7 8 9 10

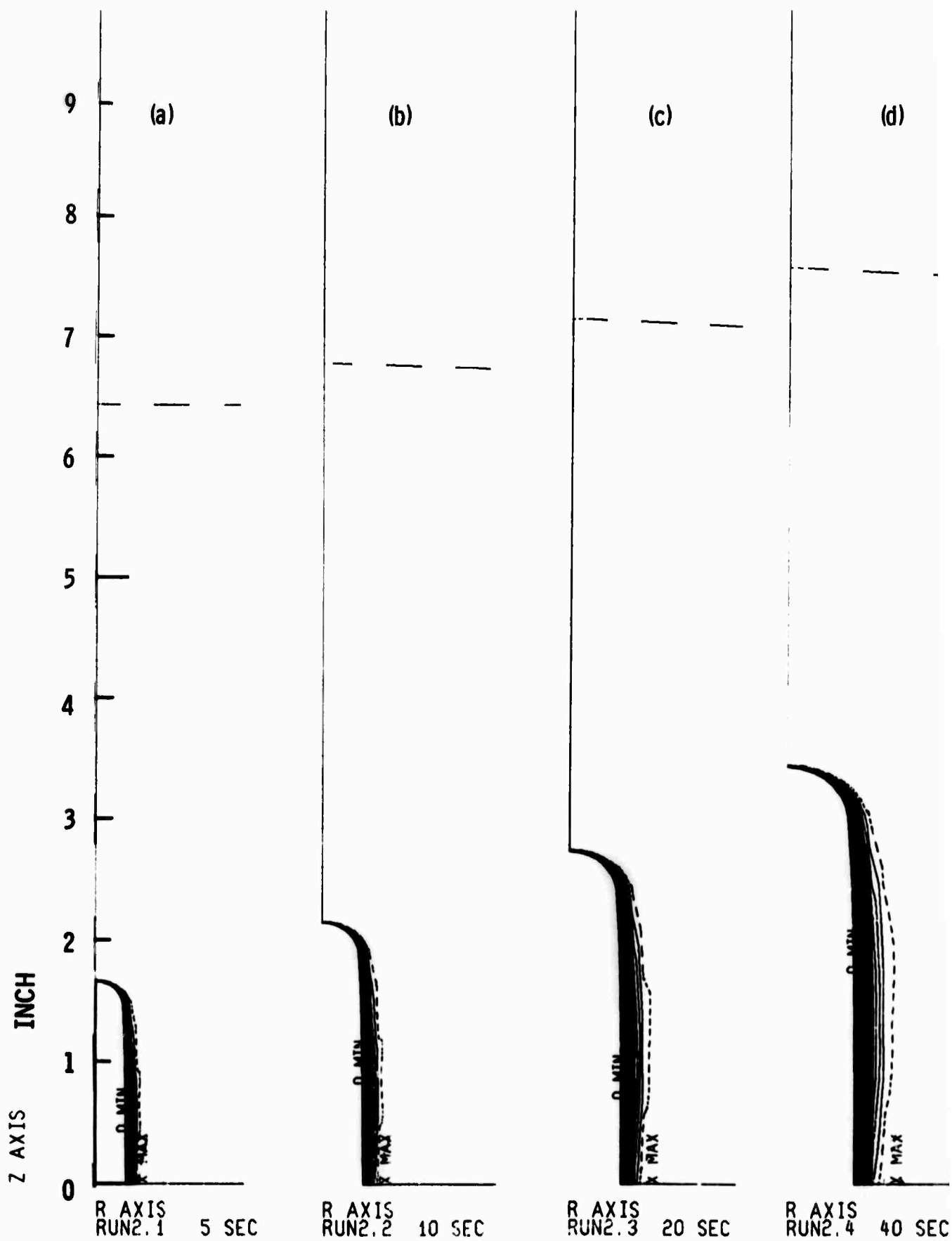
R AXIS INCH
RUN2 6 300 SEC

9 KW CYLINDRICAL BLOCK OF ROCK 20IN DIA X 10IN HIGH MAXIMUM STRESS

Figure 4-6. Calculated Maximum Principal Stress (Tension) in R-Z Plane for Piercing Times of 5, 10, 20, 40, 80, and 300 Seconds

D

a



9 KW CYLINDRICAL BLOCK OF ROCK 20IN DIA X 10IN HIGH θ STRESS

B

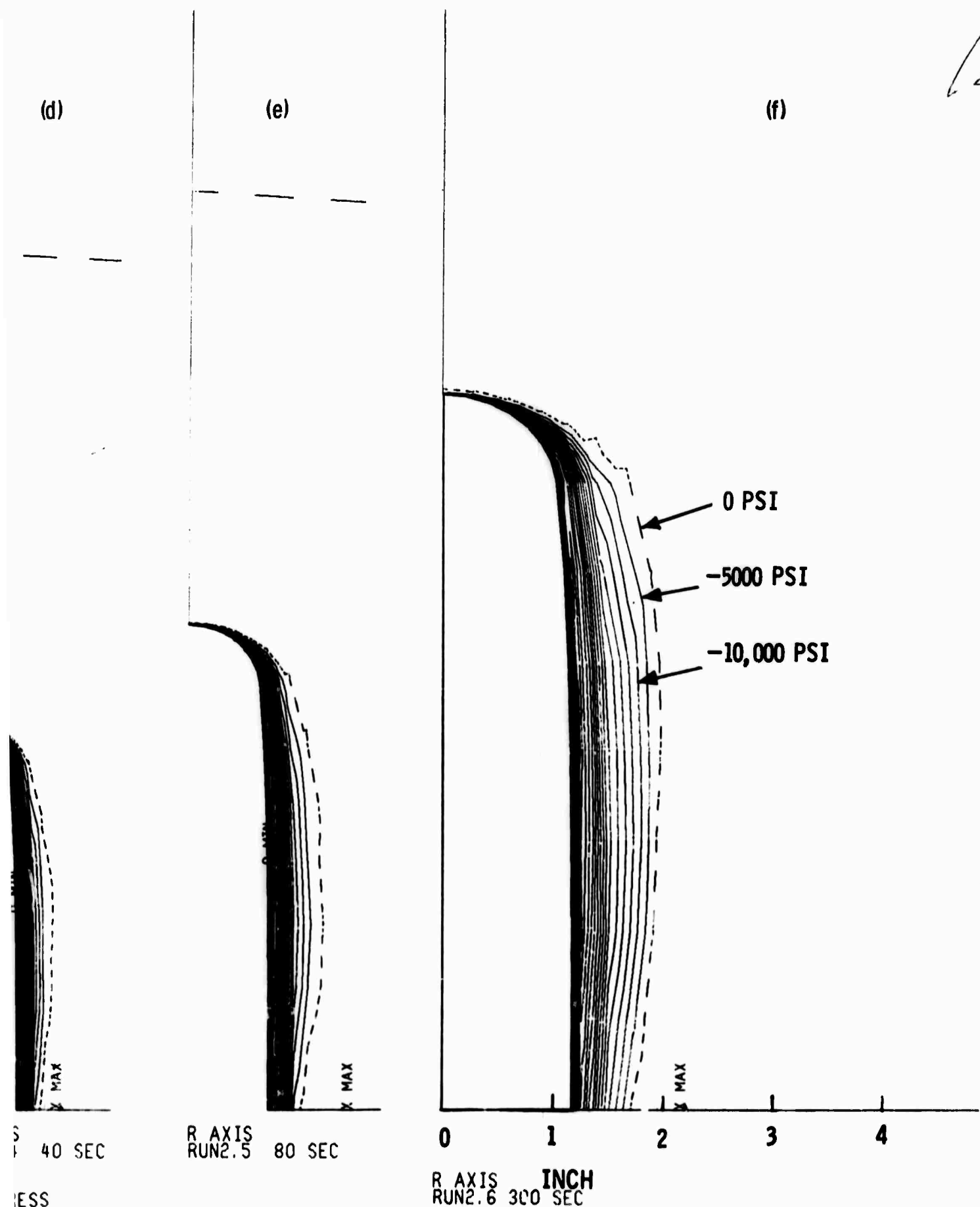
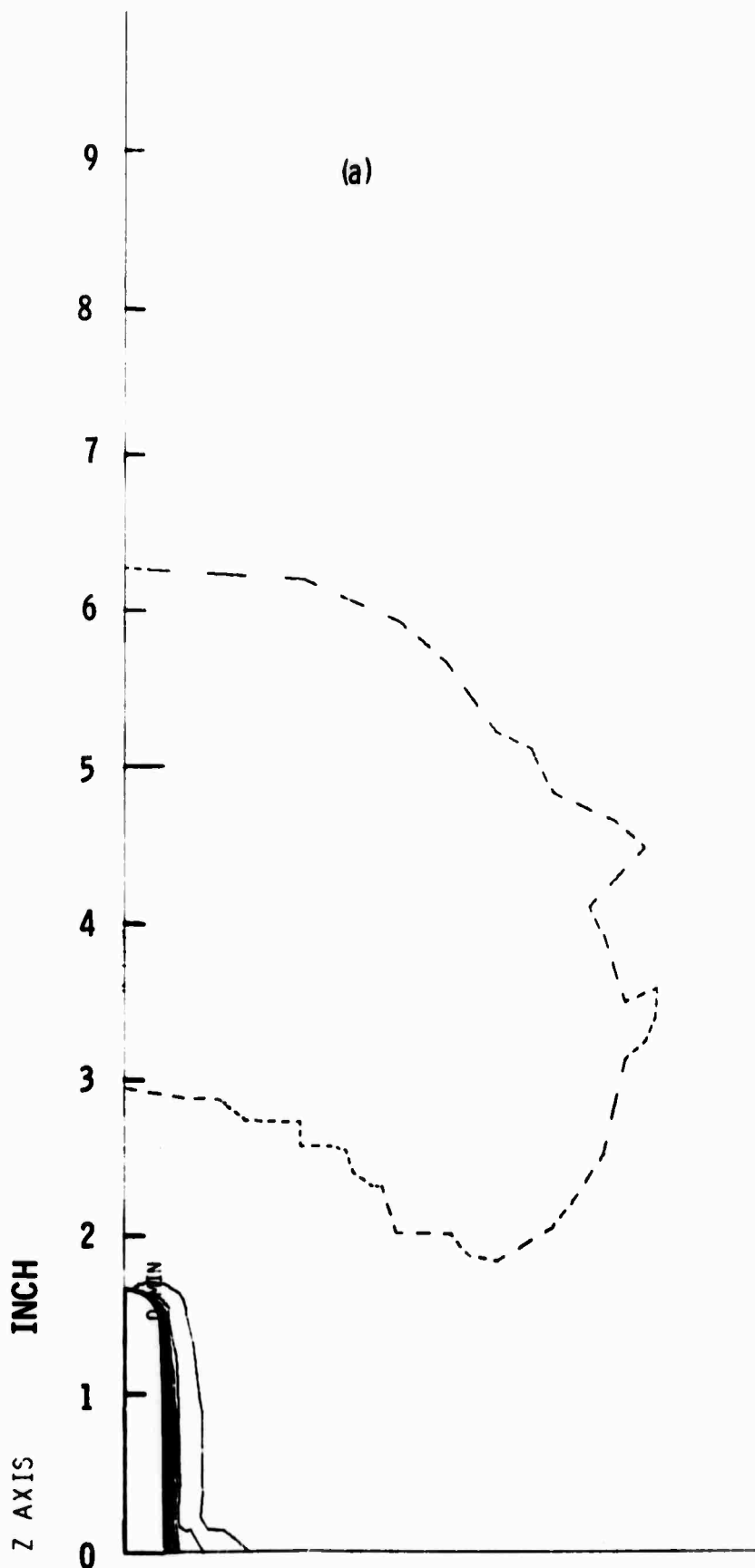


Figure 4-7. Calculated Azimuthal Compression for Piercing Times of 5, 10, 20, 40, 80, and 300 Seconds

a



(a)

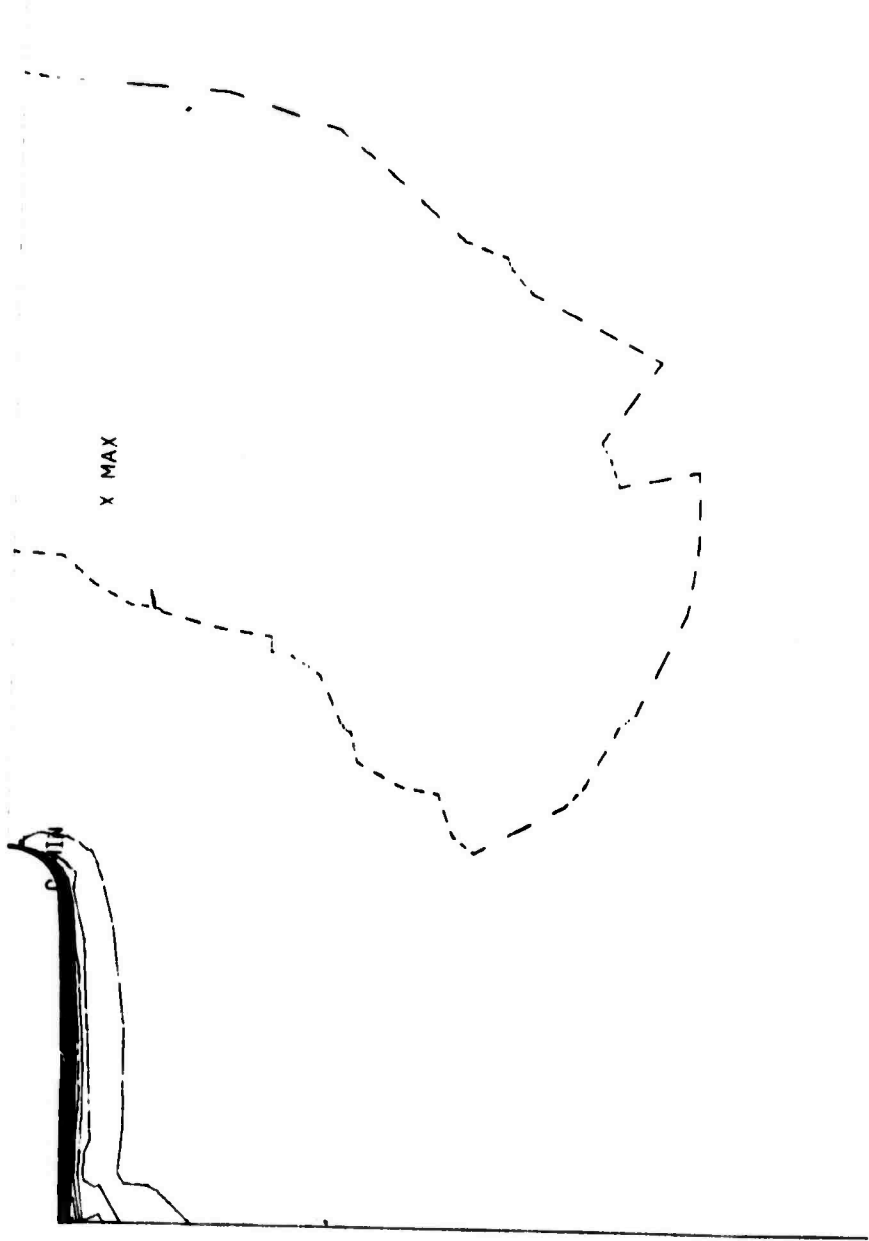
R AXIS
RUN2.1 5 SEC



R AXIS
RUN2.2

B

(b)



X MAX

R AXIS
RUN2.2 10 SEC

(c)



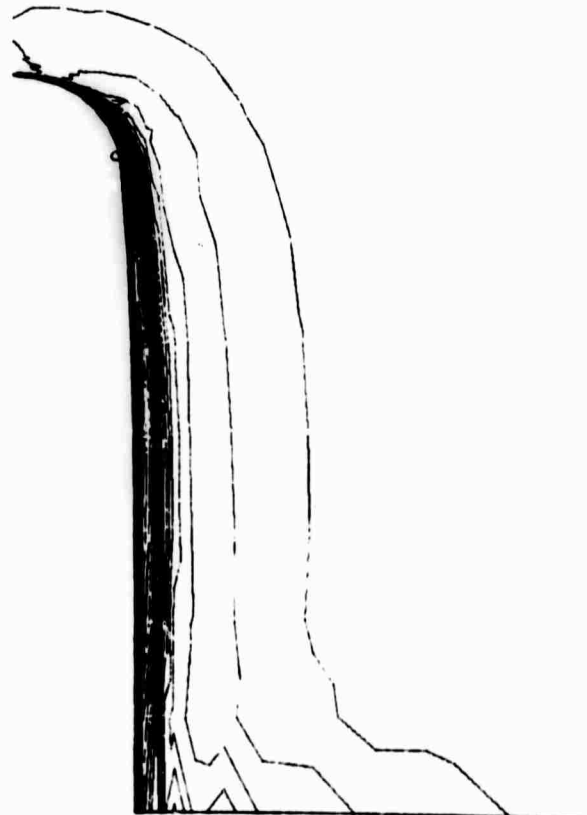
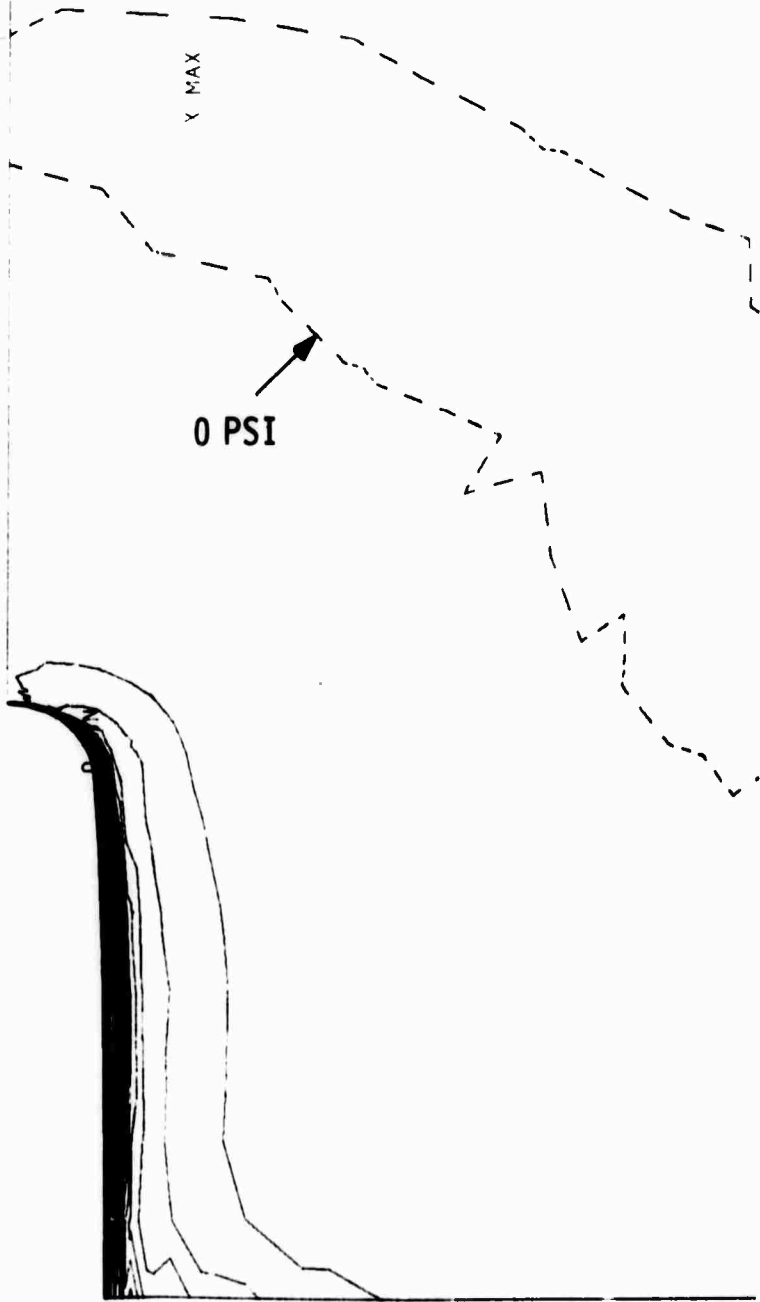
X MAX

R AXIS
RUN2.3 20 SEC

C

(d)

(e)



R AXIS
RUN 2.4 40 SEC

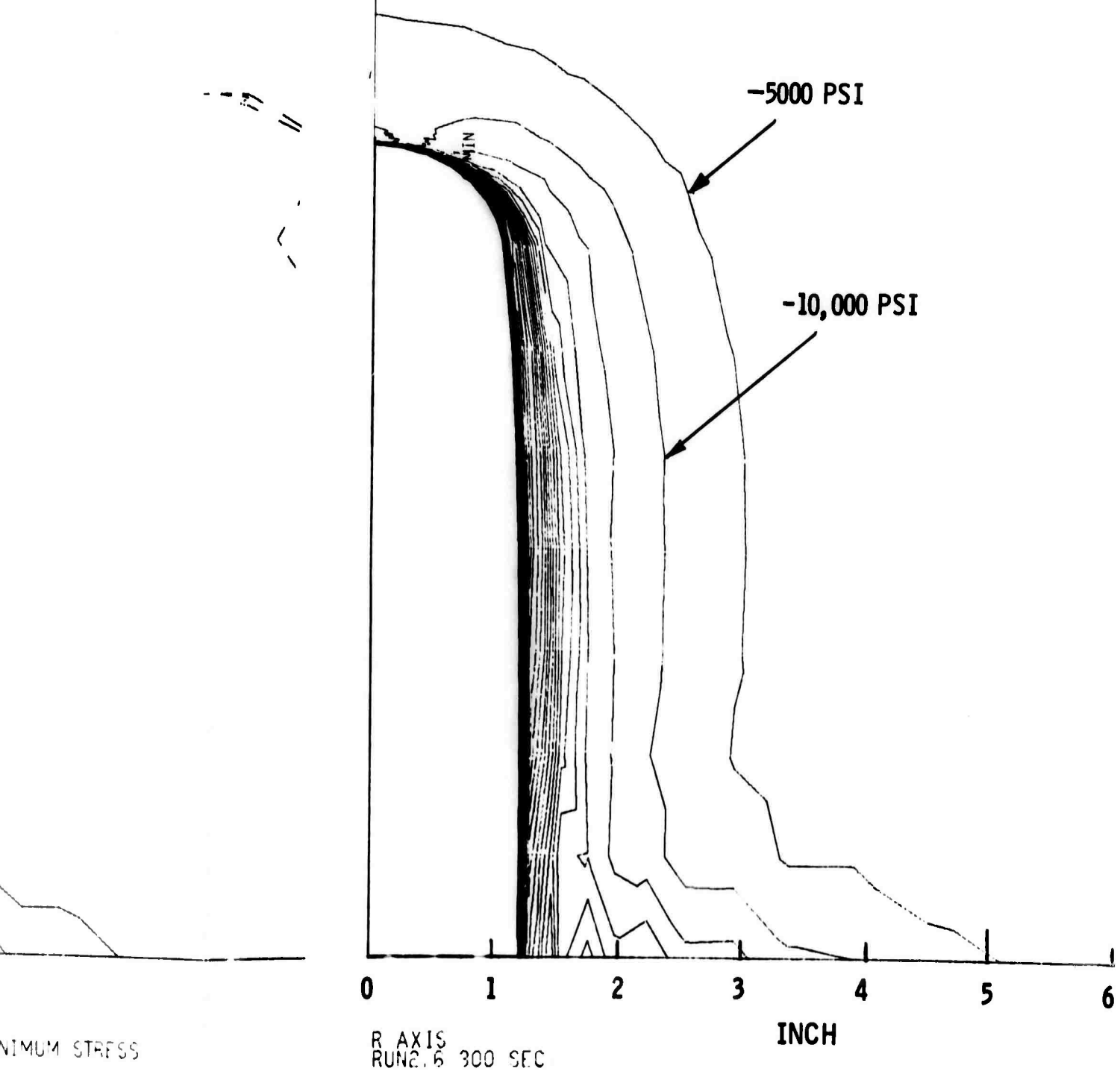
R AXIS
RUN 2.5 80 SEC

3 KW CYLINDRICAL BLOCK OF ROCK 20IN DIA X 10IN HIGH MINIMUM STRESS

(e)

D

(f)



MINIMUM STRESS

R AXIS
RUN 2.6 300 SEC

Figure 4-8. Calculated Minimum Principal Stress (Compression) in R-Z Plane for Piercing Times of 5, 10, 20, 40, 80, and 300 Seconds

Table 4-2

ELASTIC AND THERMAL PARAMETERS ASSIGNED TO EACH ELEMENT
ACCORDING TO ITS TEMPERATURE

<u>Temperature (° C)</u>	<u>Coefficient of Thermal Expansion</u>	<u>Young's Modulus (psi)</u>	<u>Poisson Ratio</u>
0-100	2.6×10^{-6}	145×10^5	0.24
100-225	6.0	141	0.23
225-350	8.2	135	0.21
350-475	10.2	126	0.19
475-600	11.2	107	0.145
600-620	11.7	83	0.105
620-640	11.8	64	0.09
640-660	11.9	46	0.07
660-680	12.0	28	0.05
680-700	12.0	9	0.02

Note: These data are similar to that for Dresser basalt in Table 4-4, page 18 of Ref. 4.

In each of the four cases there are six plots representing the six piercing times 5, 10, 20, 40, 80, and 300 seconds. For the plots of tensile stress, the contours represent 500 to 10,000 psi in 500 psi increments. For the azimuthal compressive stress, the contours represent 0 (dashed line) to -80,000 psi in -5000 psi increments. And, for the compressive principal stress, the contours represent 0 (dashed line) to -76,000 psi in -4000 psi increments. The directions of the principal stresses in the r-z plane are more or less parallel to the isostress contours.

4.6 INTERPRETATION OF STRESS FIELDS

There are several interesting qualitative features of the stress plots in Figure 4-5 through 4-8.

1. Compressive stresses and stress gradients are many times larger than tensile stresses and stress gradients, i.e., typically by one order of magnitude. (However, there is an even wider disparity between compressive strength and tensile strength; hence, the predominant failure mechanism is failure under tension.)
2. In the neighborhood of the cavity, the stresses are compressive wherever rock is heated. This compression is caused by the presence of the surrounding cold region, which restrains the thermal expansion of the hot region.
3. Outside the heated region, the rock is under tension.
 - a. The expansion of the hot region along the axis of the cavity tends to stretch the cold region in the z direction. This stress will tend to cause cracks in a plane perpendicular to the axis of the cavity.
 - b. The radial growth of the heated region causes tension in the azimuthal direction. This stress will tend to cause cracks in planes that are parallel to and contain the axis of the cavity.
4. Azimuthal tension is greater than tension in the r-z plane at depths down to those comparable to the depth of the cavity. At depths similar to that of the cavity and below, tension in the r-z plane begins to exceed azimuthal tension. Such stresses can produce failure configurations similar to those observed in laboratory experiments, namely, a combination of a vertical crack (caused by the azimuthal tension) in a plane containing the cavity

axis together with a horizontal crack (caused by the r-z tension), which cuts through the bottom of the cavity.

Figure 4-9 shows the best example available of this theory. The cavity in this block of pink Jasper quartzite is only 2 inches deep (one half the height of the block), whereas in other cases the cavity nearly penetrated blocks of this size before splitting. In these latter cases, the horizontal cracks, clearly visible in Figure 4-9, could not develop. Moreover, this quartzite is very fine grain, homogenous, and isotropic. Note also the fine cracks and the lifting of the material near the top edge of the cavity.

5. The region over which the stresses act expands with time, as one would expect. The depth of the stress field exceeds the depth of the cavity, particularly for longer piercing times.
6. For each piercing time, the calculations show nontrivial values in the cold region where the tensile stress is many times greater than a typical tensile strength of rock ($\sim 10^3$ psi).

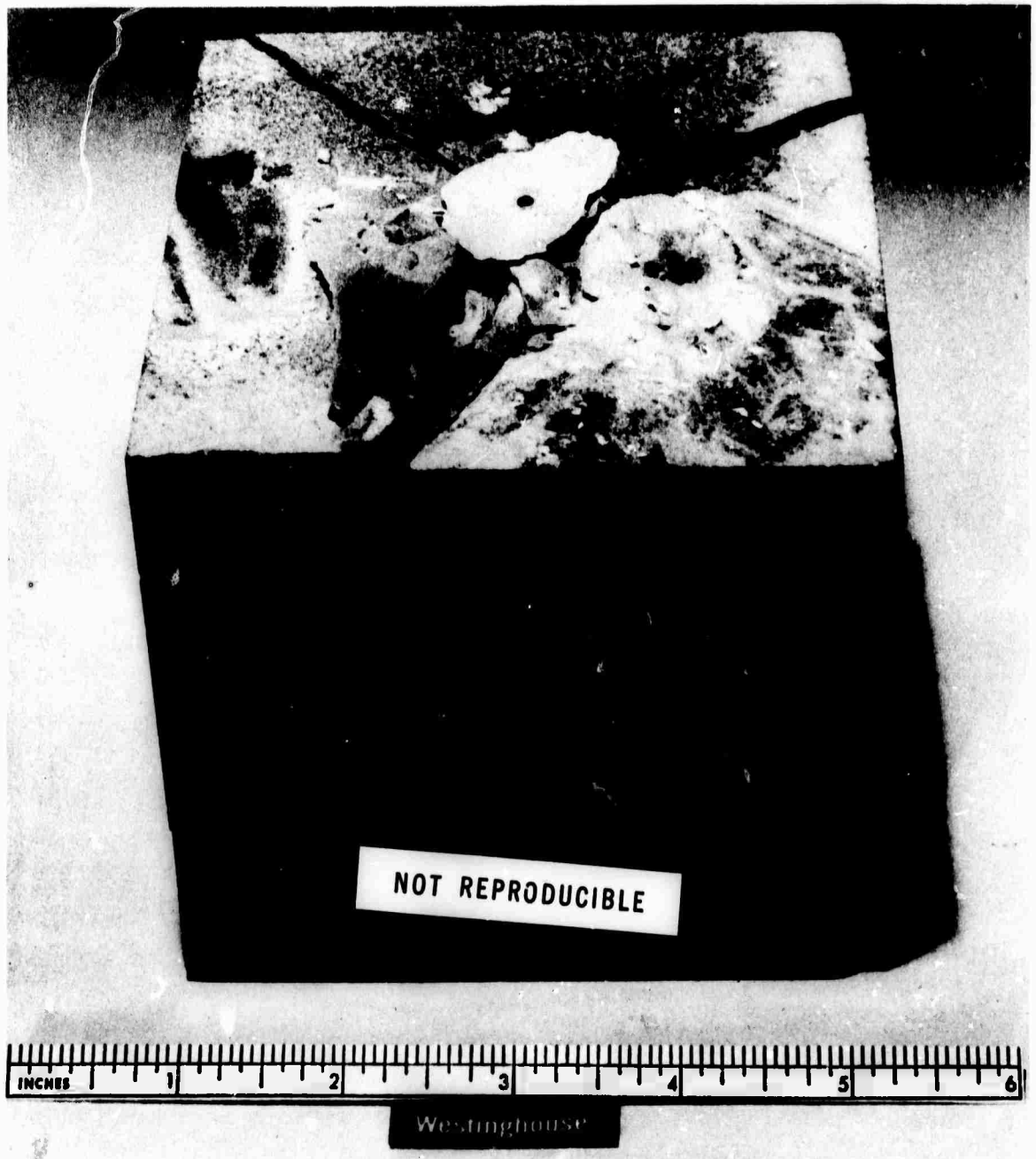


Figure 4-9. Pink Jasper Quartzite Cracked after 9 Seconds of Piercing with 9-kW Beam (from Ref. 2)

4.7 ROCK FAILURE

Although the rock is expected to fail under tension, prediction of the time, location, and configuration of the fracture surface is quite complicated. There is, in fact, no unique tensile strength for a given type of rock. For example, Jaeger and Cook (Ref. 8, p. 140) make the statement: "The tensile strength of rock is more variable and more influenced by specimen size than any other mechanical property of rock."

A useful interpretation is that the effect of size on tensile strength is statistical in nature. The larger the volume under tension, the higher the probability of initiating a failure somewhere in the volume. This is a version of the so-called "weakest link" theory. Jaeger and Cook (Ref. 8, p. 186) discuss such a formulation by Weibull (Ref. 9) which gives the probability of failure as

$$P = 1 - \exp \left[\int \ln(1-P_0) dv \right] \quad (5)$$

where dv is an element of volume and P_0 is the probability that a unit volume will fail. P_0 is a function of stress which, in turn, is a function of position. For simplicity, Weibull assumes a power law for P_0 such that P becomes (in the notation of Hudson (Ref. 10)):

$$P = 1 - \exp \left[- \int \left(\frac{s}{s_0} \right)^m dv \right] \quad (6)$$

where m and s_0 are constants depending on the type of rock, and s , a function of position, is the maximum principal tensile stress.

Although Hudson found s_0 and m to vary somewhat with volume, it is instructive to use some typical values that he obtained from measurements on red granite, i.e., $s_0 \sim 2000$, and $m=6$. Using these values together with the calculated stresses (Section 4.5), the results shown in Figure 4-10 are obtained.

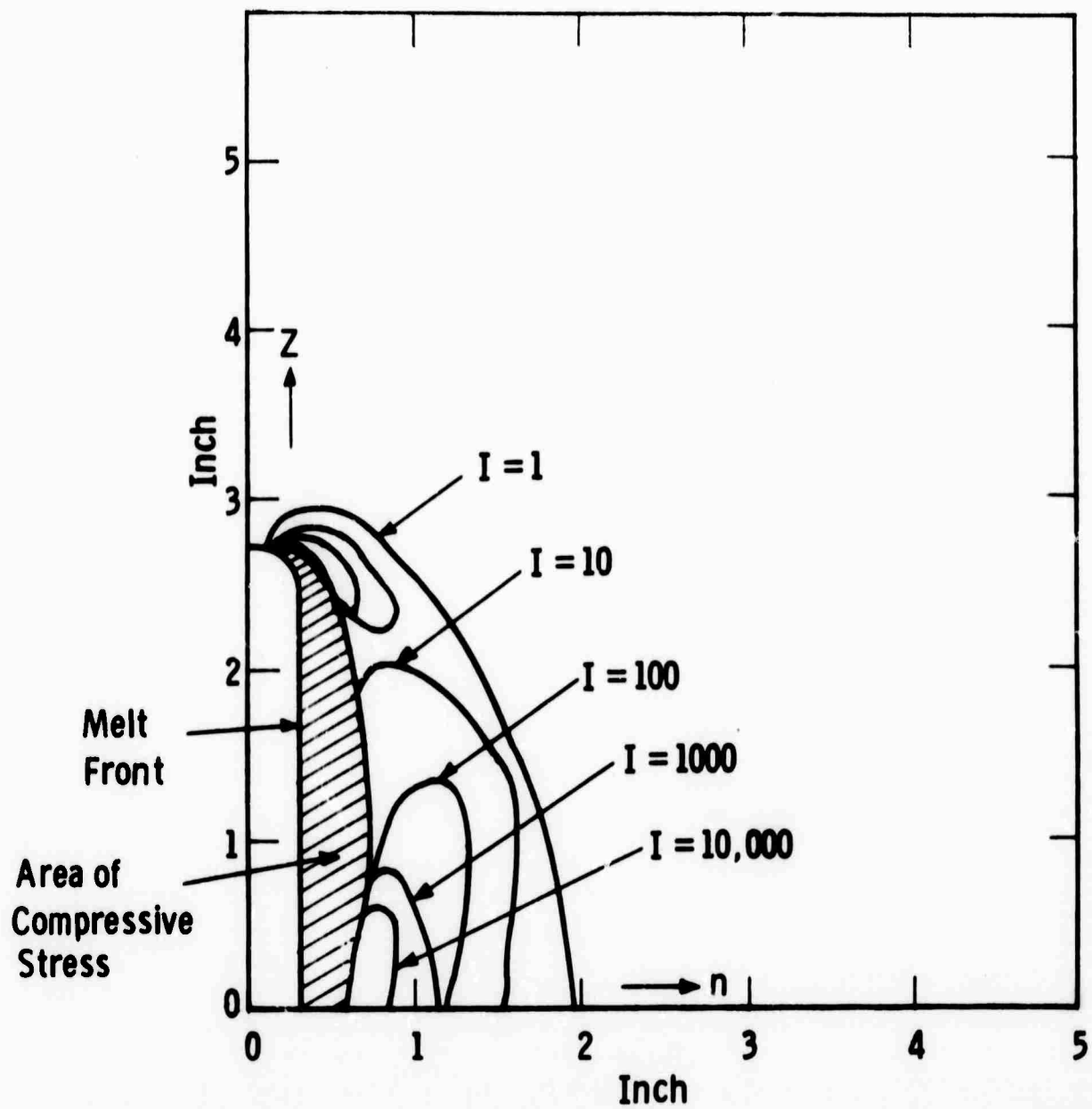


Figure 4-10. Failure Probability Due to Tensile Stresses

The contours in Figure 4-10 are of the parameter $I(r, s)$ defined by

$$I(r, s) = \left(\frac{s}{2000}\right)^6 2\pi r$$

The probability that a crack will occur in a ring of small cross section, $\Delta A = \Delta r \Delta z$ is then

$$P = 1 - \exp[-I(r, s)\Delta A]$$

The contours shown are for $I = 1$ to $I = 10,000$; these are derived from the stress plot for 20 seconds piercing time with a 9 kW, 150 kV beam.

From Figure 4-10, there are apparently large regions that are almost certain to fail after only 20 seconds of piercing time. For example, the coefficient I reaches values of 1000 and more near the top of the cavity and also near the bottom. Such very localized regions where cracks are most likely to occur may trigger the all-important crack initiation. This may happen after a very short piercing time, because of the steep temperature gradients produced by the electron-beam process.

However, under what conditions the cracks would then propagate and develop is open to question. For example, if such localized stress begins to develop early in the piercing process, a small crack could be produced and relieve the stress. Perhaps the neighborhood surrounding the small crack would subsequently be overtaken by the advancing front of molten rock. Further study of this subject will be necessary to determine the extent to which such a complicated sequence of events does occur. One would also like to know to what extent such a process would alter the temperature field, and at what point the cracks will cease to be localized and propagate far from the cavity.

On the basis of piercing tests and observations, one would expect that the larger volumes heated to lower temperatures and farther from the melt-front, as well as farther from the top surface, are responsible for propagating the large fractures, which do occur.

Graphs similar to Figure 4-10 for longer piercing times have not yet been made.

5. LABORATORY TESTS

No laboratory tests were performed during the second quarter.

6. REFERENCES

1. B. W. Schumacher, "Electron Beam Cutting of Rocks and Concrete," Electron and Ion Beam Science and Technology, Third International Conference, (R. A. Bakish, ed.); The Electrochemical Society Inc. New York 1968, pp. 447-468. Also E/MJ, June 1969, pp. 116-119.
2. B. W. Schumacher and C. R. Taylor, "Rock Breakage by Means of Electron Beam Piercing (Laboratory Tests)," Record of 10th Symposium on Electron, Ion, and Laser Beam Technology (L. Marton, ed.); San Francisco Press, Inc., 1969, pp. 271-284.
3. Westinghouse Missile Launching and Handling Dept., Sunnyvale, Calif., R 71-16, First Quarterly Technical Report (1 January - 31 March 1971) - Use of Electron Beam Gun for Hard Rock Excavation, 30 April 1971.
4. Kr. Thirumalai, Potential of Internal Heating Method for Rock Fragmentation, U.S. Bureau of Mines, Twin Cities, Minn., 1970.
5. R. B. Sosman, The Properties of Silica, The Chemical Catalog Company, Inc., New York, 1927, p. 86.
6. Kr. Thirumalai, "Process of Thermal Spalling Behavior in Rocks - An Exploratory Study," Proceedings Eleventh Symposium on Rock Mechanics, Berkeley, Calif., June 16-19, 1969, p. 709.
7. W. M. Rohsenow and H. Choi, Heat, Mass, and Momentum Transfer, Prentice-Hall, Englewood Cliffs, New Jersey, 1961, p. 123.
8. J. C. Jaeger and N.G.W. Cook, Fundamentals of Rock Mechanics, Methuen & Company, London, 1969.
9. W. Weibull, "A Statistical Theory of the Strength of Materials," Ingenjersk. Akad. Handl. No. 151.
10. J. A. Hudson, Proceedings of the Eighth Symposium on Rock Mechanics, September 15-17, 1966, The American Institute of Mining, Metallurgical, and Petroleum Engineers, Inc., New York, 1967, p. 162.